

We would like to take this opportunity to thank the editor and all reviewers for their thoughtful and constructive comments, from which our manuscript has greatly benefited. For the most part the changes that were made in response to the reviewer's comments are outline in the individual responses to reviewer's comments. All minor typos, rewording and changes to the figures have been made. Outlined below is a list of the major changes we have made to the manuscript and an instance where we found it was not possible to fulfill the request of the reviewer during revision of the manuscript.

Major issues addressed:

1) Presentation of other datasets

We have made considerable revisions to the introduction. Here, we now present the pre-existing $\delta^{11}\text{B}_{\text{sw}}$ records, focusing on the similarity between records. The discussion of these various records has been extended later in the manuscript in comparison to our new $\delta^{11}\text{B}_{\text{sw}}$. As with the introduction, we follow the referee's suggestion and the revised discussion section now clearly emphasises the similarity between the various records, building towards consensus. Only in the case of specific discrepancies between the records do we explore the differences in methodology between the $\delta^{11}\text{B}_{\text{sw}}$ reconstructions as a way to explain any of the differences.

2) More detailed discussion of uncertainties and modeling parameters.

The uncertainties used in the Monte Carlo simulation and the variables changed in the modeling studies have now been tabulated in order to improve the clarity in these sections of the manuscript. Included in the table of uncertainties is also a justification of the 2σ that we apply.

3) Simplifying the $\delta^{11}\text{B}_{\text{sw}}$ output and applying the most appropriate $\delta^{13}\text{C}/\text{pH}$ relationship

Reviewer 1 suggested that given the overlap in uncertainties between the different records we presented, it wasn't appropriate to recommend the use of one of our $\delta^{11}\text{B}_{\text{sw}}$ record over another. This valuable comment led us to re-think the presentation of our central argument with regard to the uncertainty of $\Delta\text{pH}/\Delta\delta^{13}\text{C}$ relationship and thereby, we think, both simplified and improved our study. We now present a single record that captures a broader range of different $\delta^{13}\text{C}/\text{pH}$ relationships than any of our

initial scenarios. In practical terms, this is done by applying a flat probability (ie. Equal rather than normally distributed) of ± 0.05 to the ΔpH estimate using the central $\Delta\text{pH}/\Delta\delta^{13}\text{C}$ slope of $0.175/\text{\textperthousand}$ diagnosed from our extensive sensitivity tests using both the CYCLOPS and GENIE models. This nominal uncertainty is equivalent to the broad range of $\Delta\text{pH}/\Delta\delta^{13}\text{C}$ slopes of $0.14/\text{\textperthousand}$ and $0.21/\text{\textperthousand}$ – covering the vast majority of our model simulations and removing the need to present separate “slope scenarios”. That is, because we have used a flat probability there is an equal likelihood of any value between about $0.14/\text{\textperthousand}$ and $0.21/\text{\textperthousand}$. To avoid confusion and given the evidence from our $\delta^{13}\text{C}$ data and modeling work we have also now discarded the hypothetical scenario where the pH gradient was assumed to have remained the same as modern. The second motivation for following this broad approach is that it is not possible to test the $\delta^{13}\text{C}/\text{pH}$ relationship at our specific sites as requested by reviewer 1, nor for the low latitudes. Currently pre-industrial surface water $\delta^{13}\text{C}$ data is only available for the North Atlantic $>20^\circ\text{N}$ (Olsen and Ninnemann, 2010). When a wider dataset of pre-industrial water column $\delta^{13}\text{C}$ is available in the future, it will be possible to refine our $\delta^{11}\text{B}_{\text{sw}}$ record. We now make this point explicitly.

4) Exploration of the smoothing parameter and the impact on the record

In order to test the dependence of the output record on the smoother we have undertaken a binning exercise where we have averaged our data over 8 Myr intervals. The calculated mean and two standard errors of the data in each interval show that the difference between the middle Miocene $\delta^{11}\text{B}_{\text{sw}}$ and modern is significant. The presence of the rise in $\delta^{11}\text{B}_{\text{sw}}$ across this interval in a number of other published records suggests that our record adds to the growing consensus on the evolution of $\delta^{11}\text{B}_{\text{sw}}$ in the Neogene.

1 **A record of Neogene seawater $\delta^{11}\text{B}$ reconstructed from paired $\delta^{11}\text{B}$**
2 **analyses on benthic and planktic foraminifera.**

3 Greenop Rosanna^{1,2*}, Hain, Mathis P.¹, Sosdian, Sindia M.³, Oliver, Kevin J.C.¹,
4 Goodwin, Philip¹, Chalk, Thomas B.^{1,4}, Lear, Caroline H.³, Wilson, Paul A.¹, Foster,
5 Gavin L.¹

6 *Corresponding author

7 ¹*Ocean and Earth Science, National Oceanography Centre Southampton, University
8 of Southampton, Waterfront Campus, European Way, Southampton SO14 3ZH, UK*

9 ²*School of Geography & Geosciences, Irvine Building, University of St Andrews,
10 North Street, St Andrews, KY16 9AL, UK*

11 ³*School of Earth & Ocean Sciences, Cardiff University, Cardiff, CF10 3AT, UK*

12 ⁴*Department of Physical Oceanography, Woods Hole Oceanographic Institution,
13 Woods Hole, Massachusetts, USA*

14

15 **Abstract:**

16 The boron isotope composition ($\delta^{11}\text{B}$) of foraminiferal calcite, which reflects
17 seawater pH, is a well-established proxy for reconstructing past seawater carbonate
18 chemistry and, in the case of planktic foraminifera, past atmospheric CO₂. However,
19 to translate $\delta^{11}\text{B}$ measurements determined in calcareous fossils into pH we need to
20 know the boron isotope composition of the seawater in which they grew ($\delta^{11}\text{B}_{\text{sw}}$).
21 While a number of $\delta^{11}\text{B}_{\text{sw}}$ reconstructions exist, more work is needed to build
22 confidence in our knowledge of this important parameter. Here we present a new
23 Neogene $\delta^{11}\text{B}_{\text{sw}}$ record based on the $\delta^{11}\text{B}$ difference between paired measurements of
24 planktic and benthic foraminifera and an estimate of the coeval water column pH
25 gradient derived from planktic/benthic $\delta^{13}\text{C}$ data. To underscore this approach we
26 present extensive tests using the CYCLOPS and GENIE carbon cycle models to
27 demonstrate that the planktic/benthic $\Delta\text{pH}/\Delta\delta^{13}\text{C}$ relationship is relatively insensitive
28 to ocean and carbon cycle changes. In keeping with previously published records, our
29

r.greenop 17/8/2016 17:50

Deleted: .

r.greenop 5/9/2016 11:50

Deleted: Foster, G.L.¹,

r.greenop 17/8/2016 17:50

Deleted: .

r.greenop 5/9/2016 11:51

Deleted: Hain, M.P.¹,

r.greenop 17/8/2016 17:50

Deleted: .

r.greenop 17/8/2016 17:50

Formatted: Not Superscript/ Subscript

r.greenop 17/8/2016 17:51

Deleted: planktic

r.greenop 11/8/2016 14:13

Deleted: palaeo- atmospheric CO₂ and

r.greenop 5/9/2016 11:52

Deleted: parent

r.greenop 8/6/2016 20:30

Deleted: the discrepancies between them reveals uncertainties and deficiencies that need to be addressed

r.greenop 11/8/2016 14:18

Deleted: .

r.greenop 5/9/2016 11:53

Deleted: pH gradient

r.greenop 11/8/2016 14:15

Deleted: between surface and deep water

r.greenop 11/8/2016 14:18

Deleted: We then

r.greenop 11/8/2016 14:19

Deleted: calculate $\delta^{11}\text{B}_{\text{sw}}$ two different ways. One variant of our method assumes that the pH gradient between surface and deep has remained the same as today over the past 23 Ma; the other uses the $\delta^{13}\text{C}$ gradient between surface and deep

r.greenop 11/8/2016 14:20

Deleted: to represent change in the pH gradient through time. The results of these two methods of calculating $\delta^{11}\text{B}_{\text{sw}}$ are broadly consistent with each other, however, based on extensive carbon cycle modelling using CYCLOPS and GENIE we favour the $\delta^{13}\text{C}$ gradient method.

r.greenop 8/6/2016 20:31

Deleted: In

reconstruction suggests that $\delta^{11}\text{B}_{\text{sw}}$ was $\sim 37.5\text{‰}$ during the early and middle Miocene and rapidly increased from ~ 12 to 5 Ma to reach a plateau near the modern value of 39.61‰ . A similar pattern of change is evident in the seawater composition of the Mg, Li and Ca stable isotope systems. Concurrent shifts in the seawater isotopic composition of all four of these elements during the late Miocene are suggestive of a common forcing mechanism. Based on the observed direction of change we hypothesise that an increase in secondary mineral formation during continental weathering may have affected the isotopic composition of the riverine input to the ocean since $\sim 12\text{-}15\text{ Ma}$.

1. Introduction

Key to determining the relationship between CO_2 and climate in the geological past is the calculation of reliable estimates of absolute CO_2 through time. In recent years the boron isotope composition ($\delta^{11}\text{B}$) of foraminiferal calcite has become a high-profile tool for reconstructing CO_2 beyond the last 800 kyr and throughout the Cenozoic Era (Foster, 2008; Höönsch et al., 2009; Pearson et al., 2009; Bartoli et al., 2009; Foster et al., 2012; Badger et al., 2013; Henehan et al., 2013; Greenop et al., 2014; Martínez-Botella et al., 2015a). Yet long-term change in the boron isotope composition of seawater ($\delta^{11}\text{B}_{\text{sw}}$) is currently poorly constrained and represents a major source of the uncertainty associated with $\delta^{11}\text{B}$ -determined CO_2 estimates (e.g. Pearson et al., 2009). In the modern ocean boron is a conservative element with a spatially invariant isotope ratio (39.61‰ ; Foster et al., 2010), but this value is subject to change through geological time. The residence time of boron in the ocean is estimated to lie between 11 and 17 Myrs (Lemarchand et al., 2000). Therefore we can expect the uncertainty associated with $\delta^{11}\text{B}_{\text{sw}}$ to be an important factor in CO_2 estimates beyond the late Pliocene ($\sim 4\text{-}5\text{ Ma}$, Palmer et al., 1998; Lemarchand et al., 2000; Pearson et al., 2009; Foster et al., 2012).

The ocean boron budget and its isotopic composition are controlled by a number of inputs and outputs (Fig. 1). However, because the magnitude of the boron fluxes between land, the ocean and the atmosphere in the modern are still poorly understood, the residence time and changes in both concentration ($[\text{B}]_{\text{sw}}$) and isotopic composition ($\delta^{11}\text{B}_{\text{sw}}$) through time remain uncertain. The main inputs of B into the

r.greenop 21/7/2016 10:40
Deleted: favoured $\delta^{11}\text{B}_{\text{sw}}$
r.greenop 8/6/2016 20:31
Deleted: , $\delta^{11}\text{B}_{\text{sw}}$
r.greenop 11/8/2016 14:20
Deleted: is around 2‰ lower than today at
r.greenop 11/8/2016 14:20
Deleted: and
r.greenop 11/8/2016 14:21
Deleted: increases to the modern value (39.61‰) by $\sim 5\text{ Ma}$
r.greenop 11/8/2016 14:21
Deleted: of three other stable isotope systems,
r.greenop 11/8/2016 14:23
Deleted: ,
r.greenop 11/8/2016 14:24
Deleted: suggest a common forcing mechanism. We hypothesise the most likely cause of these shifts is a change in the isotopic composition of the riverine input, potentially driven by an increase in secondary mineral formation since $\sim 15\text{ Ma}$.
r.greenop 5/9/2016 16:24
Deleted: one of the most commonly used
r.greenop 5/9/2016 16:25
Deleted: s
r.greenop 6/9/2016 11:32
Deleted: to
r.greenop 15/6/2016 21:25
Deleted: i
r.greenop 15/6/2016 21:26
Deleted: i

r.greenop 26/7/2016 19:37
Deleted: 2

115 ocean are silicate weathering delivered to the ocean by rivers (Lemarchand et al.,
116 2000), hydrothermal vents (You et al., 1993) and fluid expelled from accretionary
117 prisms (Smith et al., 1995). The major loss terms are oceanic crust alteration (Smith
118 et al., 1995), adsorption onto sediments (Spivack and Edmond, 1987) and co-
119 precipitation into carbonates (Hemming and Hanson, 1992). In case of all three
120 outputs, the light ^{10}B isotope is preferentially removed relative to ^{11}B , such that the
121 seawater $^{11}\text{B}/^{10}\text{B}$ ratio ($\delta^{11}\text{B}_{\text{sw}}$, 39.61‰) is significantly greater than that of the
122 cumulative inputs ($\delta^{11}\text{B}$ of ~10.4‰; Lemarchand et al., 2000). Our understanding of
123 the modern boron fluxes outlined above, and illustrated in Fig. 1, implies a significant
124 imbalance between inputs and outputs and consequently the poorly constrained
125 ocean-atmosphere boron fluxes may also be an important part of the ocean's modern
126 boron mass balance (Park and Schlesinger, 2002). In the context of this study,
127 however, we follow Lemarchand et al., (2000) and assume atmospheric fluxes are
128 unlikely to have varied significantly on geological timescales and therefore will not
129 be discussed further in reference to the Neogene record.

130
131 Unlike many other isotopic systems (e.g. $\delta^7\text{Li}_{\text{sw}}$, $\delta^{26}\text{Mg}_{\text{sw}}$, $\delta^{44/40}\text{Ca}_{\text{sw}}$, $\delta^{87}\text{Sr}/^{86}\text{Sr}$) to date
132 no archive has been discovered that simply records unaltered $\delta^{11}\text{B}_{\text{sw}}$. This is a result
133 of the pH-dependent boron speciation in seawater upon which the $\delta^{11}\text{B}$ -pH proxy is
134 based (Hemming & Hanson 1992) that imparts a pH dependency on the $\delta^{11}\text{B}$ of all
135 marine precipitates so far examined. Empirical reconstructions of $\delta^{11}\text{B}_{\text{sw}}$ must
136 therefore use “indirect” approaches. So far four approaches have been applied to the
137 problem (Fig. 2): (1) geochemical modeling (Lemarchand et al., 2000), (2) $\delta^{11}\text{B}$
138 analysis of halites (Paris et al., 2010), (3) measurements of benthic foraminiferal $\delta^{11}\text{B}$
139 coupled to various assumptions about past changes in ocean pH (Raitzsch and
140 Hönisch, 2013), and (4) measurements of $\delta^{11}\text{B}$ in surface and thermocline dwelling
141 foraminifera coupled with additional information on the pH gradient of the surface
142 ocean (Palmer et al., 1998; Pearson and Palmer 1999, Pearson and Palmer 2000;
143 Anagnostou et al., 2016). Geochemical modelling of the changes in the flux of boron
144 into and out of the ocean through time has been used to suggest that $\delta^{11}\text{B}_{\text{sw}}$ increased
145 from 37‰ at 60 Ma to 40‰ ± 1‰ today, driven by a combination of processes
146 including changing boron continental discharge (Lemarchand et al., 2000). In the
147 case of approach 2, while modern natural halites reflect $\delta^{11}\text{B}_{\text{sw}}$ (39.7‰) with no
148 apparent fractionation, measurement of $\delta^{11}\text{B}$ in ancient halites yield isotopic ratios

r.greenop 26/7/2016 19:37

Deleted: 2..., hydrothermal vents (Y ... [1]

r.greenop 11/8/2016 14:29

Formatted

[... [2]

r.greenop 11/8/2016 14:27

Deleted: such that seawater is isotopically heavier (39.61‰) than the inputs (which average at 10.4‰)...Our understanding ... [3]

r.greenop 11/8/2016 14:59

Formatted: Space After: 12 pt, No widow/orphan control, Don't adjust space between Latin and Asian text, Don't adjust space between Asian text and numbers

r.greenop 11/8/2016 14:38

Formatted

[... [4]

r.greenop 11/8/2016 14:35

Deleted: Mg, Ca, Li, Sr... to date no ... [5]

204 that are significantly lower than all other approaches (Fig. 2; Paris et al., 2010), with
 205 implausible variability among samples of the same age (7‰ range), thereby casting
 206 doubt over the reliability of this approach (Raitzsch and Höönsch, 2013). In the case
 207 of approach 3, $\delta^{11}\text{B}_{\text{sw}}$ is calculated from globally distributed benthic $\delta^{11}\text{B}$ data with an
 208 imposed degree of deep-ocean pH change (Fig. 2; Raitzsch and Höönsch, 2013). This
 209 method hinges on two key assumptions: (a) a near linear surface water pH increase of
 210 0.39 over the past 50 Myrs taken from the intermediate pH output from two modeling
 211 studies (Berner and Kothavala, 2001; Tyrrell and Zeebe, 2004; Ridgwell, 2005), and
 212 (b) a prescribed constant surface-to-deep ocean pH gradient of 0.3 (Tyrrell and
 213 Zeebe, 2004, and modern observations). The modeled surface pH and estimated fixed
 214 pH gradient is then used to estimate deep ocean pH, and then convert benthic
 215 foraminiferal $\delta^{11}\text{B}$ measurements to $\delta^{11}\text{B}_{\text{sw}}$. This approach yields broadly similar
 216 results to geochemical modeling (Fig. 2). The fourth approach exploits the non-linear
 217 relationship between $\delta^{11}\text{B}$ and pH alongside estimated pH gradients in the ocean to
 218 constrain $\delta^{11}\text{B}_{\text{sw}}$ (Palmer et al., 1998; Pearson and Palmer 1999, Pearson and Palmer
 219 2000) and is the basis of the approach used in this study. The advantage of this
 220 method is that $\delta^{11}\text{B}_{\text{sw}}$ can be reconstructed empirically without relying on dependent
 221 pH constraints. The non-linear relationship between $\delta^{11}\text{B}$ and pH means that the pH
 222 difference between two $\delta^{11}\text{B}$ data points varies as a function of $\delta^{11}\text{B}_{\text{sw}}$ (Fig. 3).
 223 Consequently, if the size of the pH gradient can be estimated then there is only one
 224 $\delta^{11}\text{B}_{\text{sw}}$ value that is consistent with the foraminiferal $\delta^{11}\text{B}$ measurements and the
 225 specified pH gradient irrespective of the absolute pH (Fig. 3c). Previously this
 226 approach has been applied to pH variations in the surface ocean and used in studies
 227 of Cenozoic $p\text{CO}_2$ to account for changes in $\delta^{11}\text{B}_{\text{sw}}$ (determined using $\delta^{11}\text{B}$ in surface
 228 and thermocline-dwelling foraminifera) (Fig. 2) (Palmer et al., 1998; Pearson and
 229 Palmer 1999, Pearson and Palmer 2000; Anagnostou et al., 2016). This approach uses
 230 a constant pH gradient between the surface and some depth proximal to the oxygen
 231 minimum zone and the boron isotope values of a mixed layer dwelling species and
 232 thermocline dweller to calculate a value for $\delta^{11}\text{B}_{\text{sw}}$ (Pearson and Palmer, 1999). The
 233 resulting record suggests that $\delta^{11}\text{B}_{\text{sw}}$ varies between 37.7‰ and 39.4‰ through the
 234 Neogene (Fig. 2) (Pearson and Palmer, 2000).
 235 The same method, but using planktic-benthic instead of surface planktic- thermocline
 236 planktic $\delta^{11}\text{B}$ gradients to calculate $\delta^{11}\text{B}_{\text{sw}}$, was recently applied to the middle

r.greenop 11/8/2016 14:52
Deleted: Results from studies employing this method
r.greenop 8/6/2016 21:00
Deleted: suggest that $\delta^{11}\text{B}_{\text{sw}}$ has varied by 7‰ over the Neogene (Fig. 2)
r.greenop 11/8/2016 14:54
Deleted: (Paris et al., 2010)
r.greenop 8/6/2016 21:01
Deleted: Yet brine-halite fractionation offsets of -20‰ to -30‰ and -5‰ are reported from laboratory and natural environments respectively casting doubt over the validity of the assumption that no fractionation occurs during halite formation (Vengosh et al., 1992; Liu et al., 2000). These fractionations and riverine input during basin isolation will drive the evaporate-hosted boron to low- $\delta^{11}\text{B}$ isotope values such that the fluid inclusion record likely provides a lower limit for the $\delta^{11}\text{B}_{\text{sw}}$ through time (i.e. $\delta^{11}\text{B}_{\text{sw}}$ is heavier than the halite fluid inclusions of Paris et al. (2010)). Nevertheless, evaporites form from modified seawater in isolated basins making them ... [6]
r.greenop 11/8/2016 14:53
Deleted: An alternative semi-empiric ... [7]
r.greenop 5/9/2016 13:57
Deleted: assumes
r.greenop 11/8/2016 14:55
Deleted: 1
r.greenop 11/8/2016 14:55
Deleted: 2
r.greenop 5/9/2016 13:58
Deleted:
r.greenop 5/9/2016 13:58
Deleted:
r.greenop 11/8/2016 14:56
Deleted: which can be converted to $\delta^{11}\text{B}$... [8]
r.greenop 18/7/2016 15:00
Deleted: While this approach yields a ... [9]
r.greenop 11/8/2016 14:59
Deleted: record empirically is deter ... [10]
r.greenop 11/8/2016 15:00
Deleted: One way to avoid using ab ... [11]
r.greenop 5/9/2016 16:36
Deleted: , irrespective of absolute pH,
r.greenop 18/7/2016 14:56
Deleted: .
r.greenop 5/9/2016 14:08
Deleted: The resultant curve produced by t
r.greenop 5/9/2016 16:37
Deleted: his method
r.greenop 5/9/2016 14:08
Deleted: shows
r.greenop 18/7/2016 12:14
Moved down [3]: Unfortunately, t ... [12]

348 Miocene where it yielded a $\delta^{11}\text{B}_{\text{sw}}$ of $37.6^{+0.4}_{-0.5}$ ‰ (Foster et al., 2012). A further
349 modification to the method of Pearson and Palmer (1999) was also proposed in that
350 study wherein $\delta^{13}\text{C}$ in foraminiferal calcite was used to estimate the surface-to-deep
351 pH gradient (Foster et al., 2012). Here, we reconstruct $\delta^{11}\text{B}_{\text{sw}}$ for the last 23 Ma, the
352 Neogene, based on this modified approach. We undertake extensive sensitivity tests
353 using both the CYCLOPS carbon cycle box model and the GENIE Earth system
354 model to define the plausible range in the relationship between surface/deep pH
355 difference and $\delta^{13}\text{C}$ difference, which is an essential parameter for this approach.
356 Finally, we employ a Monte Carlo approach for comprehensive propagation of
357 uncertainty in all input parameters and we focus on reconstructing $\delta^{11}\text{B}_{\text{sw}}$ – the
358 implications of our work for understanding the evolution of Neogene ocean pH and
359 atmospheric $p\text{CO}_2$ will be documented elsewhere.

360 2. Methods

361 2.1 Site Locations and Age Models

362 Foraminifera from four sites are used to construct the planktic-benthic $\delta^{11}\text{B}$ pairs;
363 Ocean Drilling Program, ODP, Site 758 and ODP Site 999 for the Pleistocene and
364 Pliocene samples and ODP Site 926 and Site 761 for the Miocene (Fig. 4) (this study;
365 Foster et al., 2012; Martínez-Botí et al., 2015a, Sosdian et al., *in prep*). We also
366 incorporate the middle Miocene planktic-benthic pair from Site 761 in Foster et al.,
367 (2012). To place all data from all sites on a single age model, we use the nanno and
368 planktic foraminifera stratigraphy from sites 999, 926 and 761 (Shipboard Scientific
369 Party, 1997; Shipboard Scientific Party, 1995; Zeeden et al., 2013; Holbourn et al.,
370 2004) updated to GTS2012 (Gradstein et al., 2012). At Site 758 the
371 magnetostratigraphy (Shipboard Scientific Party, 1989) is used and updated to
372 GTS2012 (Gradstein et al., 2012).

373 2.2 Boron Isotope Analysis and pH Calculation

374 The boron isotope measurements (expressed in delta notation as $\delta^{11}\text{B}$ – permil
375 variation) were made relative to the boric acid standard SRM 951; (Catanzaro et al.,
376 1970). Boron was first separated from the Ca matrix prior to analysis using the boron

r.greenop 11/8/2016 15:13

Deleted: The major limitation of these pH gradient approaches is the assumption of a constant pH gradient through time. A useful extension to this method therefore utilises the

r.greenop 11/8/2016 18:05

Deleted:

r.greenop 11/8/2016 18:05

Deleted: and then determine $\delta^{11}\text{B}_{\text{sw}}$

r.greenop 11/8/2016 18:05

Deleted: Here we expand on the study of Foster et al. (2012) and present a number of new $\delta^{11}\text{B}_{\text{sw}}$ records based on $\delta^{11}\text{B}$ measured in planktic-benthic pairs. In our first treatment of the data we assume that the pH gradient has remained the same as modern at each site through time. In the second approach we utilise benthic-planktic $\delta^{13}\text{C}$ gradients to correct for changes in the pH gradient. Using a biogeochemical box model and an Earth system model we also assess the extent to which the relationship between pH and $\delta^{13}\text{C}$ gradients has remained constant under a comprehensive range of hypothetical carbon system and oceanographic states. We also use this model output to determine which pH/ $\delta^{13}\text{C}$ regression is most appropriate for our data. In this study we focus on reconstructing $\delta^{11}\text{B}_{\text{sw}}$, whereas implications of our record in terms of the evolution of Neogene ocean pH and atmospheric $p\text{CO}_2$ are documented in a follow up study (Sosdian et al., *submitted*).

r.greenop 5/9/2016 14:14

Deleted: Martinez-Botí

r.greenop 6/9/2016 11:39

Deleted: submitted

r.greenop 5/9/2016 14:09

Deleted:,

r.greenop 5/9/2016 16:51

Deleted: In order to put all the sites

r.greenop 5/9/2016 16:51

Deleted: at

r.greenop 5/9/2016 16:52

Deleted: Site

r.greenop 5/9/2016 16:52

Deleted: Site

r.greenop 5/9/2016 16:52

Deleted: the biostratigraphy is used from

r.greenop 6/9/2016 11:40

Deleted:),(

r.greenop 6/9/2016 11:40

Deleted:) and (

r.greenop 6/9/2016 11:40

Deleted: respectively and

417 specific resin Amberlite IRA 743 following Foster et al. (2013). The boron isotopic
418 composition was then determined using a sample-standard bracketing routine on a
419 ThermoFisher Scientific Neptune multicollector inductively coupled plasma mass
420 spectrometer (MC-ICPMS) at the University of Southampton (following Foster et al.,
421 2013). The relationship between $\delta^{11}\text{B}$ of $\text{B}(\text{OH})_4^-$ and pH is very closely
422 approximated by the following equation:

$$pH = pK_B^* - \log \left(- \frac{\delta^{11}\text{B}_{\text{SW}} - \delta^{11}\text{B}_{\text{CaCO}_3}}{\delta^{11}\text{B}_{\text{SW}} - \alpha_B \cdot \delta^{11}\text{B}_{\text{CaCO}_3} - 1000 \cdot (\alpha_B - 1)} \right) \quad (1)$$

423

424 Where pK_B^* is the equilibrium constant, dependent on salinity, temperature, pressure
425 and seawater major ion composition (i.e., [Ca] and [Mg]), α_B is the fractionation
426 factor between the two boron species and $\delta^{11}\text{B}_{\text{sw}}$ is the boron isotope composition of
427 seawater. [Here we use the fractionation factor of 1.0272, calculated from](#)
428 [spectrophotometric measurements \(Klochko et al., 2006\)](#). [No temperature correction](#)
429 [was applied as a number of recent studies suggest that it is not significant over our](#)
430 [investigated temperature range \(Rae et al. 2011; Henehan et al., 2013; Martínez-Botí](#)
431 [et al. \(2015b\); Kaczmarek et al. 2016\)](#). Although the $\delta^{11}\text{B}$ of foraminifera correlates
432 well with pH and hence $[\text{CO}_2]_{\text{aq}}$, the $\delta^{11}\text{B}_{\text{calcite}}$ is often not exactly equal to $\delta^{11}\text{B}_{\text{borate}}$
433 (Sanyal et al., 2001; Foster, 2008; Henehan et al., 2013). The planktic species used to
434 construct the benthic-planktic pairs changes through time, as a single species is not
435 available for the entire Neogene (this study; Foster et al., 2012; Martínez-Botí et al.,
436 2015a, Sosdian et al., [in prep](#)). Here *Globigerinoides ruber* is used for 0 to 3 Ma,
437 *Trilobatus sacculifer* (formally *Globigerinoides sacculifer* and including *Trilobatus*
438 *trilobus*; Hembleden et al., 1987; Spezzaferri et al., 2015) for 0 to 20 Ma and
439 *Globigerina praebulloides* for 22 to 23 Ma. The calibration for *G. ruber* (300-
440 355 μm) [is derived from culturing data supported by core top data \(Henehan et al.](#)
441 [2013\). The *T. sacculifer* calibration \(300-355 \$\mu\text{m}\$ \) is from Sosdian et al., \(\[in prep\]\(#\)\)](#)
442 where the *T. sacculifer* calibration of Sanyal et al., (2001) is used with a modified
443 intercept so that it passes through the core top value for *T. sacculifer* (300–355 μm)
444 from ODP Hole 999A (Seki et al., 2010). Unlike the symbiotic modern *G. bulloides*,
445 *G. praebulloides* appears to be symbiotic at least in the latest Oligocene (Pearson and
446 Wade, 2009). Therefore, we apply the *T. sacculifer* (300-355 μm) calibration to this

r.greenop 5/9/2016 14:12

Formatted: Space After: 12 pt, No widow/orphan control, Don't adjust space between Latin and Asian text, Don't adjust space between Asian text and numbers

r.greenop 5/9/2016 14:12

Formatted: Font:Times, 12 pt

r.greenop 6/9/2016 11:41

Deleted: submitted

r.greenop 11/8/2016 18:07

Deleted: is from Henehan et al., (2013)

r.greenop 6/9/2016 11:41

Deleted: submitted

r.greenop 6/9/2016 11:42

Deleted: T

451 species. For *T. sacculifer* (500-600µm) between 0 and 1 Ma, we use the calibration
452 from Martínez-Botí et al. (2015b) where the calibration of Sanyal et al. (2001)
453 measured using NTIMS is corrected for the offset between MC-ICPMS and NTIMS
454 using a comparison of core-top *T. sacculifer* measured by the two different methods
455 from adjacent sites (Foster, 2008; Sanyal et al., 1995). In order to constrain deep-
456 water pH, analysis was conducted on benthic foraminifera *Cibicidoides wuellestorfi*
457 or *Cibicidoides mundulus* depending on which species were most abundant in each
458 sample. The $\delta^{11}\text{B}$ of both *Cibicidoides* species shows no offset from the theoretical
459 $\delta^{11}\text{B}$ of the borate ion and therefore no calibration is needed to adjust for species-
460 specific offsets (Rae et al., 2011).

r.greenop 15/6/2016 21:50

Deleted: at 0.7 Ma

r.greenop 11/8/2016 18:11

Deleted:,

r.greenop 5/9/2016 14:12

Formatted: Font:Times

461 As mentioned above, in addition to $\delta^{11}\text{B}_{\text{calcite}}$, temperature, salinity, water depth
462 (pressure) and seawater major ion composition are also needed to calculate pH from
463 $\delta^{11}\text{B}$. We use the MyAMI specific ion interaction model (Hain et al., 2015) to
464 calculate the appropriate equilibrium constants based on existing [Ca] and [Mg]
465 reconstructions (Horita et al., 2002; Brennan et al., 2013). Sea surface temperature
466 (SST) is calculated from tandem Mg/Ca analyses on an aliquot of the $\delta^{11}\text{B}$ sample
467 (with a conservative 2σ uncertainty of 2°C). Adjustments were made for changes in
468 Mg/Ca_{sw} using the records of Horita et al. (2002) and Brennan et al. (2013), and
469 correcting for changes in dependence on Mg/Ca_{sw} following Evans and Muller (2012)
470 using H = 0.41 calculated from *T. sacculifer* (where H describes the power
471 relationship between test Mg/Ca incorporation and Mg/Ca_{sw}; Delaney et al., 1985;
472 Hasiuk and Lohmann, 2010; Evans and Muller, 2012) using the equations:

$$\text{Mg/Ca}_{\text{sw},c} = (\text{Mg/Ca}_{\text{sw},a} / \text{Mg/Ca}_{\text{sw},m})^{0.41} \quad (2)$$

473 Where Mg/Ca_{sw,c} is the correction factor applied to the temperature equation for
474 changing Mg/Ca_{sw}, Mg/Ca_{sw,a} is the estimated Mg/Ca_{sw} for the age of the sample and
475 Mg/Ca_{sw,m} is modern Mg/Ca_{sw}. Temperature is then calculated using the generic
476 planktic foraminifera calibration of Anand et al. (2003) and including a correction
477 factor for Mg/Ca_{sw}.

r.greenop 5/9/2016 14:12

Formatted: Font:Times

r.greenop 5/9/2016 14:12

Formatted: Font:(Asian) Japanese,
(Other) English (US)

r.greenop 13/7/2016 16:24

Deleted: planktic foraminifera

$$\text{Temperature} = \ln(\text{Mg/Ca}_{\text{test}} / (0.38 * \text{Mg/Ca}_{\text{sw},c})) / 0.09 \quad (3)$$

478 Mg/Ca analysis was conducted on a small aliquot of the sample dissolved for isotope
479 analysis at the University of Southampton using a ThermoFisher Scientific Element 2

483 XR. Al/Ca was also measured to assess the competency of the sample cleaning.
484 Because of complications with the Mg/Ca-temperature proxy in *Cibicidoides* species
485 (Elderfield et al., 2006), bottom water temperatures (BWTs) are estimated here by
486 taking the global secular temperature change from the Mg/Ca temperature
487 compilation of Cramer et al. (2011), using the calibration of Lear et al. (2010) and
488 applying this change to the modern bottom water temperature at each site taken from
489 the nearest GLODAP site (with a conservative 2σ uncertainty of 2°C). Salinity is held
490 constant at modern values determined from the nearest GLODAP site (2σ uncertainty
491 of 2 ‰ uncertainty) for the entire record. Note that temperature and salinity have
492 little influence on the calculated pH and the uncertainty in $\delta^{11}\text{B}_{\text{sw}}$ is dominated by the
493 uncertainty in the $\delta^{11}\text{B}$ measurement and the estimate of the pH gradient.

494 The majority of the $\delta^{13}\text{C}$ data were measured at Cardiff University on a
495 ThermoFinnigan MAT 252 coupled with a Kiel III carbonate device for automated
496 sample preparation. Additional samples were measured on a gas source mass
497 spectrometer Europa GEO 20-20, University of Southampton equipped with
498 automated carbonate preparation device and on a Finnigan MAT 253 gas isotope
499 ratio mass spectrometer connected to a Kiel IV automated carbonate preparation
500 device at the Zentrum für Marine Tropenökologie (ZMT), Bremen. The Pliocene
501 benthic $\delta^{13}\text{C}$ from Site 999 were taken from the nearest sample in Haug and
502 Tiedemann, (1998). In almost all cases $\delta^{13}\text{C}$ was analysed on the same foraminiferal
503 species as $\delta^{11}\text{B}$ and Mg/Ca (38/44 samples). Where this was not possible another
504 surface dweller/benthic foraminifera was used from the same depth habitat. *C. wuellestorfi* or *C. mundulus* were measured in all cases for benthic $\delta^{13}\text{C}$. Stable
505 isotope results are reported relative to the Vienna PeeDee belemnite (VPDB)
506 standard. We use a carbon isotope vital effect for *G. ruber* (+0.94 ‰; Spero et al.,
507 2003), *T. sacculifer/G. praebulloides* (+0.46 ‰; Spero et al., 2003; Al-Rousan et al.,
508 2004);, *C. mundulus* (+0.47 ‰; McCorkle et al., 1997) and *C. wuellestorfi* (+0.1 ‰;
509 McCorkle et al., 1997) to calculate the $\delta^{13}\text{C}$ of dissolved inorganic carbon (DIC).

511 2.3 Carbon isotopes as a proxy for vertical ocean pH gradient

512 The use of $\delta^{13}\text{C}$ in foraminiferal calcite to estimate the surface to deep pH gradient
513 requires knowledge of the slope of the pH- $\delta^{13}\text{C}$ relationship in the past. In this section

r.greenop 5/9/2016 14:17

Deleted: National Oceanography Centre
Southampton (USNOCs)

r.greenop 5/9/2016 14:17

Deleted: was

r.greenop 13/7/2016 16:18

Deleted: An adjustment for vital effects on
the $\delta^{13}\text{C}$ of

r.greenop 6/9/2016 11:44

Deleted: is applied

520 | we briefly outline the main factors that contribute to the pH- $\delta^{13}\text{C}$ relationship in order
521 to underpin our analysis of extensive carbon cycle model simulations.

r.greenop 15/7/2016 11:01

Deleted: s

522 The production, sinking and sequestration into the ocean interior of low- $\delta^{13}\text{C}$ organic
523 carbon via the soft-tissue component of the biological pump (e.g., Hain et al., 2014a)
524 | leads to a broad correlation between $\delta^{13}\text{C}$, $[\text{CO}_3^{2-}]$ and macronutrients in the ocean.
525 The remineralization of this organic matter decreases $\delta^{13}\text{C}$ and titrates $[\text{CO}_3^{2-}]$ so as to
526 reduce pH, while nutrient concentrations are increased. In waters that have
527 experienced more soft tissue remineralization both pH and $\delta^{13}\text{C}$ will be lower (Fig.
528 | 5a,b), which is the dominant cause for the positive slope between $\delta^{13}\text{C}$ and pH in the
529 modern ocean (e.g., Foster et al., 2012; Fig. 5c).

r.greenop 21/7/2016 10:08

Deleted: 4

r.greenop 21/7/2016 10:08

Deleted: 4

530 Another significant factor affecting the spatial distribution of both $\delta^{13}\text{C}$ and pH is
531 seawater temperature, which affects both the equilibrium solubility of DIC and the
532 equilibrium isotopic composition of DIC. Warmer ocean waters have decreased
533 equilibrium solubility of DIC and so increased local $[\text{CO}_3^{2-}]$ and pH (Goodwin and
534 Lauderdale, 2013), while warmer waters have relatively low equilibrium $\delta^{13}\text{C}$ values
535 (Lynch-Stieglitz et al, 1995). This means that a spatial gradient in temperature acts to
536 drive $\delta^{13}\text{C}$ and pH in opposite directions: warmer waters tend to have higher pH but
537 lower $\delta^{13}\text{C}$. These opposing temperature effects act to reduce the pH difference
538 between two points with greatly different temperature to below the value expected
539 based on $\delta^{13}\text{C}$ alone. That is, when using $\delta^{13}\text{C}$ differences to estimate the pH gradient
540 between the warm low latitude surface and cold deep waters the appropriate pH- $\delta^{13}\text{C}$
541 relationship will be less than expected when only considering the effect of the
542 biological pump. For this reason, in our modeling analysis we focus on the warm-
543 surface to cold-bottom $\Delta\text{pH}/\Delta\delta^{13}\text{C}$ rather than the slope of the overall pH- $\delta^{13}\text{C}$
544 relationship, with the latter expected to be greater than the former.

545 In the modern ocean, and for the preceding tens of millions of years, the two
546 dynamics described above are likely dominant in setting spatial variation in $\delta^{13}\text{C}$ and
547 pH (and $[\text{CO}_3^{2-}]$). However, other processes will have a minor effect on either pH or
548 | $\delta^{13}\text{C}$. For instance, the dissolution of CaCO_3 shells increases $[\text{CO}_3^{2-}]$ and pH
549 (Broecker and Peng, 1982), but does not significantly affect $\delta^{13}\text{C}$ (Zeebe and Wolf-
550 Gladrow, 2001). Moreover, the long timescale of air/sea isotopic equilibration of CO_2

r.greenop 11/8/2016 18:14

Deleted: se

r.greenop 11/8/2016 18:15

Deleted: processes

r.greenop 15/7/2016 11:04

Deleted: accumulation of remineralized

r.greenop 15/7/2016 11:04

Deleted: hard-tissue

558 | combined with kinetic isotope fractionation during net carbon transfer is an important
559 factor in setting the distribution of $\delta^{13}\text{C}$ on a global ocean scale (Galbraith et al.,
560 | 2015; Lynch-Stieglitz et al., 1995), while the effect of CO₂ disequilibrium on [CO₃²⁻]
561 and pH is modest (Goodwin and Lauderdale, 2013).
562

r.greenop 5/9/2016 14:28

Deleted: . The surface

r.greenop 5/9/2016 14:28

Deleted: also has a substantial effect on $\delta^{13}\text{C}$ (Lynch-Stieglitz et al., 1995) while it affects

r.greenop 5/9/2016 14:29

Deleted: only marginally

563 2.4 Modelling the pH to $\delta^{13}\text{C}$ relationship

564 | After correcting for the shift in $\delta^{13}\text{C}$ due to anthropogenic activity, or Suess effect
565 | (Keeling 1979), modern ocean observations demonstrate a near linear relationship
566 between global ocean data of seawater *in situ* pH and $\delta^{13}\text{C}$ DIC with a slope of
567 | 0.201±0.005 (2 σ) (Foster et al., 2012; Fig 5c.) This empirically determined slope
568 might well have been different in past oceans with very different nutrient cycling,
569 carbon chemistry and circulation compared to today, and it does not appropriately
570 represent the temperature effect described above (i.e., warm-surface to cold-bottom
571 water $\Delta\text{pH}/\Delta\delta^{13}\text{C}$). Here we use an ensemble approach with two independent carbon
572 cycle models to investigate changes in the $\Delta\text{pH}/\Delta\delta^{13}\text{C}$ regression. Below we provide
573 pertinent information on the GENIE and CYCLOPS model experiments:

r.greenop 6/9/2016 11:46

Deleted:)

574 We use the Earth System model GENIE-1 (Edwards and Marsh, 2005; Ridgwell et al.
575 | 2007) to assess the robustness of the pH-to- $\Delta\delta^{13}\text{C}$ relationship and its sensitivity to
576 physical and biogeochemical ocean forcing. The configuration used here is closely
577 related to that of Holden et al. (2013), in which the controls on oceanic $\delta^{13}\text{C}$
578 distribution were assessed, with an energy and moisture balance in the atmosphere,
579 simple representations of land vegetation and sea ice, and frictional geostrophic
580 ocean physics. In each of 16 vertical levels in the ocean, increasing in thickness with
581 depth, there are 36x36 grid cells (10° in longitude and nominally 5° in latitude, with
582 higher resolution at low latitudes). Modern ocean bathymetry and land topography is
583 applied in all simulations. The ocean biogeochemical scheme (Ridgwell et al. 2007)
584 is based on conversion of DIC to organic carbon associated with phosphate uptake
585 with fixed P:C:O stoichiometry. Organic carbon and nutrients are remineralized
586 according to a remineralization profile with a pre-defined *e*-folding depth scale. This
587 depth scale, as well as the rain ratio of inorganic to organic carbon in sinking
588 particulate matter, is among the parameters examined in the sensitivity study. In these

r.greenop 21/7/2016 11:18

Deleted: show that the

r.greenop 11/8/2016 18:17

Deleted: pH to $\delta^{13}\text{C}$ slope can only have changed in very tight limits

r.greenop 11/8/2016 18:17

Deleted: pH- $\delta^{13}\text{C}$

r.greenop 5/9/2016 16:54

Deleted: the

r.greenop 5/9/2016 16:54

Deleted: n's

600 simulations, there is no interaction with sediments. As a result of this, the steady state
601 solutions reported here are reached within the 5000-year simulations, but are not
602 consistent with being in secular steady state with regard to the balance of continental
603 weathering and ocean CaCO_3 burial.

r.greenop 5/9/2016 16:55
Deleted: a
r.greenop 11/8/2016 18:18
Deleted: is obtained
r.greenop 11/8/2016 18:18
Deleted: ;
r.greenop 11/8/2016 18:19
Deleted: the results presented here are for the end of the simulations

604 The sensitivity study consists of seven sets of experiments, each varying a single
605 model parameter relative to the control simulation with preindustrial atmospheric
606 $p\text{CO}_2$. This enables us to assess which processes, if any, are capable of altering the
607 ocean's ΔpH -to- $\Delta\delta^{13}\text{C}$ relationship, and the uncertainty in the predictive skill of this
608 relationship due to spatial variability. These experiments are therefore exploratory in
609 nature and intended to study plausible range rather than determine magnitude of past
610 changes. The seven parameters varied are (1) the ocean alkalinity reservoir; (2) the
611 ocean's carbon reservoir; (3) the parameter "S. Lim gas exchange" which blocks air-
612 sea gas exchange south of the stated latitude, significant here because of the
613 dependence of $\delta^{13}\text{C}$ on surface disequilibrium (Galbraith et al., 2015); (4) inorganic
614 to organic carbon rain ratio, controlling the relationship between DIC and alkalinity
615 distributions; (5) "Antarctic shelf FWF", a freshwater flux adjustment (always
616 switched off in control experiments with GENIE) facilitating the formation of brine
617 rich waters, which produces a high-salinity poorly-ventilated deep ocean at high
618 values; (6) "Atlantic-Pacific FWF", a freshwater flux adjustment equivalent to
619 freshwater hosing, leading to a shut-down of the Atlantic meridional overturning
620 circulation at low values; (7) remineralization depth-scale of sinking organic matter,
621 which affects the vertical gradient both of pH and $\delta^{13}\text{C}$. A wide range of parameter
622 values is chosen for each parameter in order to exceed any plausible changes within
623 the Cenozoic.

r.greenop 5/9/2016 14:29
Deleted: both
r.greenop 11/8/2016 18:19
Deleted: $\text{pH-}\delta^{13}\text{C}$
r.greenop 11/8/2016 18:20
Deleted: not
r.greenop 11/8/2016 18:19
Deleted: represent real changes that may have occurred
r.greenop 5/9/2016 16:56
Deleted: n's

624 For the second exploration of the controls on the slope of ΔpH - $\Delta\delta^{13}\text{C}$ relationship we
625 use the CYCLOPS biogeochemical 18-box model that includes a dynamical
626 lysocline, a subantarctic zone surface box and a polar Antarctic zone box (Sigman et
627 al., 1998; Hain et al., 2010, 2014b). The very large model ensemble with 13,500
628 individual model scenarios is designed to capture the full plausible range of (a)
629 glacial/interglacial carbon cycle states by sampling the full solution space of Hain et
630 al. (2010), and (b) reconstructed secular changes in seawater [Ca] (calcium
631 concentration), carbonate compensation depth (CCD), weathering and atmospheric

r.greenop 5/9/2016 14:29
Deleted: test

644 | CO₂ (Table 1). The following seven model parameters are systematically sampled to
645 set the 13,500 model scenarios: (1) shallow versus deep Atlantic meridional
646 overturning circulation represented by modern reference north Atlantic deep water
647 (NADW) versus peak glacial North Atlantic intermediate water (GNAIW)
648 circulation; (2) iron driven changes in nutrient drawdown in the subantarctic zone of
649 the Southern Ocean; (3) changes in nutrient drawdown of the polar Antarctic; (4)
650 changes in vertical exchange between the deep Southern Ocean and the polar
651 Antarctic surface; (5) range in seawater [Ca] concentration from 1x to 1.5x modern as
652 per reconstructions (Horita et al., 2002); (6) Pacific CCD is set to the range of 4.4-4.9
653 km via changes in the weathering flux, as per sedimentological evidence (Pälike et
654 al., 2012); (7) atmospheric CO₂ is set from 200 ppm to 1000 ppm by changes in the
655 ‘weatherability’ parameter of the silicate weathering mechanism. The ensemble spans
656 predicted bulk ocean DIC between 1500 and 4500 μmol/kg, a wide range of ocean
657 pH and CaCO₃ saturation states consistent with the open system weathering cycle,
658 and widely different states of the ocean’s biological pump. All 13,500 model
659 scenarios are run for two million years after every single ‘weatherability’ adjustment,
660 part of the CCD inversion algorithm, guaranteeing the specified CCD depth and
661 steady state with regard to the balance of continental weathering and ocean CaCO₃
662 burial for the final solution (unlike the GENIE simulations CaCO₃ burial was entirely
663 neglected due to computational cost of the long model integrations it would require).
664 The inverse algorithm typically takes at least ten steps to conversion, resulting in
665 ~300 billion simulated years for this ensemble.

666 2.5 Assessing uncertainty

667 δ¹¹B_{sw} uncertainty was calculated using a Monte Carlo approach where pH was
668 calculated for deep and surface waters at each time slice using a random sampling
669 (n=10000) of the various input parameters within their respective uncertainties as
670 represented by normal distributions. These uncertainties (2σ uncertainty in
671 parentheses) are: temperature (± 2 °C), salinity (±2 units on the practical salinity
672 scale) [Ca] (± 4.5 mmol/kg), [Mg], (± 4.5 mmol/kg), δ¹¹B_{planktic} (± 0.15-0.42 ‰) and
673 δ¹¹B_{benthic} (± 0.21-0.61 ‰). For the estimate of the surface to sea floor pH gradient we
674 use the central value of the Δ pH-to-Δδ¹³C relationship diagnosed from our
675 CYCLOPS and GENIE sensitivity experiments (i.e., 0.175/‰, see section 3.2 below)

r.greenop 11/8/2016 18:21

Deleted: ,

r.greenop 11/8/2016 18:21

Deleted: ,

678 and then we assign a ± 0.05 uncertainty range with a uniform probability (rather than
679 a normal distribution) to the resulting surface to sea floor ΔpH estimate (see also
680 Table 2). Thus, the magnitude of this nominal uncertainty is equivalent to a 0.14‰
681 to 0.21‰ $\Delta\text{pH}/\Delta\delta^{13}\text{C}$ uncertainty range that spans the vast majority of our
682 CYCLOPS and GENIE simulations, and the prediction error (RMSE) of fitting a
683 linear relationship to the GENIE pH and $\delta^{13}\text{C}$ output (see section 3.2 below). The
684 uncertainty in the $\delta^{11}\text{B}$ measurements is calculated from the long-term reproducibility
685 of Japanese Geological Survey *Porites* coral standard (JCP; $\delta^{11}\text{B}=24.3\text{\textperthousand}$) at the
686 University of Southampton using the equations:

687 $2\sigma = 2.25 \exp^{-23.01[\text{$_{^{11}\text{B}$}]}] + 0.28 \exp^{-0.64[\text{$_{^{11}\text{B}$}]}]}$ (4)

688 $2\sigma = 33450 \exp^{-168.2[\text{$_{^{11}\text{B}$}]}] + 0.311 \exp^{-1.477[\text{$_{^{11}\text{B}$}]}]}$ (5)

689 where $[\text{$_{^{11}\text{B}$}]$ is the intensity of ^{11}B signal in volts and equation (4) and equation (5)
690 used with $10^{11} \Omega$ and $10^{12} \Omega$ resistors, respectively.

691 From the 10,000 Monte Carlo ensemble solutions of our 22 benthic-planktic pairs we
692 construct 10,000 randomized records of $\delta^{11}\text{B}_{\text{sw}}$ as a function of time. Each of these
693 randomized $\delta^{11}\text{B}_{\text{sw}}$ records are subjected to smoothing using the locally weighted
694 scatterplot smoothing (LOWESS) algorithm with a smoothing parameter (span) of
695 0.7. The purpose of the smoothing is to put some controls on the rate at which the
696 resulting individual Monte Carlo $\delta^{11}\text{B}_{\text{sw}}$ records are allowed to change, which in
697 reality is limited by the seawater boron mass balance (~0.1 ‰ per million years;
698 boron residence time is 11–17 million years; Lemarchand et al., 2000). Our choice of
699 smoothing parameter allows for some of the individual Monte Carlo records to
700 change as fast as ~1 ‰ per million years, although in reality the average rate of
701 change is much smaller than this (see section 3.3). Consequently this method
702 removes a significant amount of uncorrelated stochastic noise (resulting from the
703 uncertainty in our input parameters) while not smoothing away the underlying signal.
704 As a result of anomalously low $\delta^{11}\text{B}$ differences (< 1‰) between benthic and planktic
705 pairs, two pairs at 8.68 Ma and 19 Ma were discarded from the smoothing. It may be
706 possible that preservation is not so good within these intervals in the core and the
707 planktic foraminifera are affected by partial dissolution (Seki et al., 2010). The
708 spread of the ensemble of smoothed $\delta^{11}\text{B}_{\text{sw}}$ curves represents the combination of the

r.greenop 11/8/2016 18:21

Deleted: and either the fixed modern pH gradient at that site (± 0.05 pH units) or the pH gradient predicted by the $\delta^{13}\text{C}$ -pH relationship (± 0.05 pH units). In our first approach we assume the pH gradient at each site has remained the same as modern through time (gradient estimated from GLODAP; Key et al., 2004). In the second approach the pH gradient is corrected using the $\delta^{13}\text{C}$ gradient (where the slope of the relationship between pH and $\delta^{13}\text{C}$ is taken from the CYCLOPS model).

r.greenop 15/7/2016 16:41

Formatted: Line spacing: 1.5 lines

r.greenop 12/8/2016 14:40

Deleted:

r.greenop 12/8/2016 14:40

Deleted: is

r.greenop 11/8/2016 18:22

Deleted: ,

r.greenop 11/8/2016 18:22

Deleted: which prevent

r.greenop 11/8/2016 18:22

Deleted: s the

r.greenop 5/9/2016 14:32

Deleted: smoothed $\delta^{11}\text{B}_{\text{sw}}$

r.greenop 12/8/2016 14:41

Deleted: from changing faster

r.greenop 12/8/2016 14:41

Deleted: than allowed

r.greenop 26/7/2016 19:38

Deleted: 2

r.greenop 5/9/2016 15:03

Formatted: Font:Times, 12 pt

r.greenop 11/8/2016 18:24

Deleted: T

730 compounded, propagated uncertainties of the various inputs (i.e., Monte Carlo
731 sampling) with the additional constraint of gradual $\delta^{11}\text{B}_{\text{sw}}$ change over geological
732 time imposed by the inputs and outputs of boron to the ocean and the total boron
733 inventory (i.e., the smoothing of individual Monte Carlo members). Various statistical
734 properties (i.e., mean, median, standard deviation (σ), various quantiles) of this
735 $\delta^{11}\text{B}_{\text{sw}}$ reconstruction were evaluated from the ensemble of smoothed $\delta^{11}\text{B}_{\text{sw}}$ records.
736 Generally, for any given benthic-planktic pair the resulting $\delta^{11}\text{B}_{\text{sw}}$ estimates are not
737 perfectly normally distributed and thus we use the median as the metric for the
738 central tendency (i.e., placement of marker in Figure 10).

r.greenop 5/9/2016 15:03
Deleted: and

r.greenop 5/9/2016 15:03
Deleted: .

739 3. Results and Discussion

740 3.1 $\delta^{11}\text{B}$ benthic and planktic data

741 Surface and deep-ocean, $\delta^{11}\text{B}$, $\delta^{13}\text{C}$ and temperature broadly show a similar, but
742 inverse, pattern to one another throughout the Neogene (Fig. 6). The $\delta^{11}\text{B}$ benthic
743 record decreases from $\sim 15\text{‰}$ at 24 Ma to a minimum of 13.28‰ at 14 Ma before
744 increasing to $\sim 17\text{‰}$ at present day (Fig. 6). This pattern and the range of values in
745 benthic foraminiferal $\delta^{11}\text{B}$ is in keeping with previously published Neogene $\delta^{11}\text{B}$
746 benthic records measured using NTIMS (Raitzsch and Hönisch, 2013), suggesting
747 that our deep-water $\delta^{11}\text{B}$ record is representative of large scale pH changes in the
748 global ocean. While the surface $\delta^{11}\text{B}_{\text{planktic}}$ remained relatively constant between 24
749 and 11 Ma at $\sim 16\text{‰}$, there is a significant increase in $\delta^{11}\text{B}$ between the middle
750 Miocene and present (values increase to $\sim 20\text{‰}$) (Fig. 6b). The reconstructed surface
751 water temperatures show a long-term decrease through the Neogene from $\sim 28^\circ\text{C}$ to
752 24°C , aside from during the Miocene Climatic Optimum (MCO) where maximum
753 Neogene temperatures are reached (Fig. 6c). Following Cramer et al. (2011) deep-
754 water temperatures decrease from $\sim 12^\circ\text{C}$ to 4°C at the present day and similarly show
755 maximum temperatures in the MCO. Surface and deep-water $\delta^{13}\text{C}_{\text{DIC}}$ both broadly
756 decrease through the Neogene and appear to covary on shorter timescales (Fig. 6e, f).

r.greenop 21/7/2016 10:08
Deleted: 5

r.greenop 21/7/2016 10:08
Deleted: 5

r.greenop 5/9/2016 15:06
Deleted:

r.greenop 21/7/2016 11:20
Deleted: $\delta^{11}\text{B}_{\text{borate}}$

r.greenop 11/8/2016 18:25
Deleted:

r.greenop 11/8/2016 18:25
Deleted:

r.greenop 21/7/2016 10:08
Deleted: 5

r.greenop 11/8/2016 18:25
Deleted:

r.greenop 21/7/2016 10:08
Deleted: 5

r.greenop 11/8/2016 18:25
Deleted:

r.greenop 21/7/2016 10:08
Deleted: 5

r.greenop 11/8/2016 18:25
Deleted:

r.greenop 21/7/2016 10:08
Deleted: 5

r.greenop 11/8/2016 18:25
Deleted:

r.greenop 21/7/2016 10:08
Deleted: 5

771 **3.2 The relationship between $\delta^{13}\text{C}$ and pH gradients**

772 As noted above, in the global modern ocean data, after accounting for the
773 anthropogenic carbon, the empirical relationship between *in situ* pH and DIC $\delta^{13}\text{C}$ is
774 well described by a linear function with a slope of 0.201 ± 0.005 (2σ) (Fig. 5; Foster
775 et al., 2012). However, this slope is only defined by surface waters in the North
776 Atlantic due to a current lack of modern data where the impact of the Suess effect has
777 been corrected (Olsen and Ninneman, 2010). Consequently we are not currently able
778 to determine the slope between the warm-surface and cold-deep ocean in the modern
779 ocean at our sites. Instead, here we use the two modeling experiments to define this
780 slope. In the control GENIE experiment (green star; Fig. 7), the central value for the
781 slope of the pH/ $\delta^{13}\text{C}$ relationship is slightly greater than 0.2‰ for the full 3D data
782 regression (not shown) and about 0.175‰ for the warm-surface-to-cold-deep ΔpH -
783 to- $\Delta\delta^{13}\text{C}$ relationship (Fig. 7) – consistent with theory for the effect of temperature
784 gradients (see section 2.3). For both ways of analysing the GENIE output the
785 prediction uncertainty of the regressions, the root-mean-squared error (RMSE), is
786 $\sim 0.05\text{‰}$ under most conditions (open red circles in Fig. 7), with the exception of
787 where large changes in either DIC or ALK result in somewhat larger changes in the
788 relationship between pH and $\delta^{13}\text{C}$ (see below). In our CYCLOPS model ensemble,
789 the central value of the slopes of the full 3D pH/ $\delta^{13}\text{C}$ regressions and of the warm-
790 surface-to-cold-deep $\Delta\text{pH}/\Delta\delta^{13}\text{C}$ is 0.2047‰ (1σ of 0.0196‰ ; Fig. 8a) and
791 0.1797‰ (1σ of 0.0213‰ ; Fig. 8b), respectively. If we restrict our analysis of the
792 CYCLOPS ensemble to only the Atlantic-basin warm-surface-to-cold-deep
793 $\Delta\text{pH}/\Delta\delta^{13}\text{C}$, where most of our samples come from, we find a relationship of only
794 0.1655‰ (1σ of 0.0192‰ ; Fig. 8c). That is, overall, we find near-perfect agreement
795 between modern empirical data and our GENIE and CYCLOPS experiments.
796 Encouraged by this agreement we select the warm-surface-to-cold-deep $\Delta\text{pH}/\Delta\delta^{13}\text{C}$
797 central value of 0.175‰ to estimate the surface/sea floor pH difference from the
798 planktic/benthic foraminifera $\delta^{13}\text{C}$ difference. To account for our ignorance as to the
799 accurate value of $\Delta\text{pH}/\Delta\delta^{13}\text{C}$ in the modern ocean, its changes over the course of the
800 study interval and the inherent prediction error from using a linear ΔpH -to- $\Delta\delta^{13}\text{C}$
801 relationship we assign a nominal uniform uncertainty range of ± 0.05 around the
802 central ΔpH estimate for the purpose of Monte Carlo uncertainty propagation. Our

r.greenop 5/9/2016 15:06

Deleted: 1

r.greenop 21/7/2016 10:08

Deleted: 4

r.greenop 15/7/2016 16:15

Deleted: and in all experiments in which ocean-physics parameters (Antarctic shelf FWF and Atlantic-Pacific FWF) are varied

r.greenop 12/8/2016 10:39

Deleted: pH/ $\delta^{13}\text{C}$ gradient is slightly greater than 0.2 , with a root-mean-squared error (RMSE) of ~ 0.05 in a reconstruction of the spatial distribution of pH using this relationship (Fig. 6).

813 analysis also suggests that where surface-to-thermocline planktic/planktonic gradients
814 are employed, the plausible $\Delta\text{pH}/\Delta\delta^{13}\text{C}$ range should be significantly higher than
815 applied here, in order to account for the relatively lower temperature difference.
816 Based on the appropriate $\Delta\text{pH}/\Delta\delta^{13}\text{C}$ relationship we reconstruct a time varying
817 surface to deep pH gradient, which ranges between 0.14 and 0.35 pH units over our
818 study interval (Fig. 9) and apply a flat uncertainty of ± 0.05 . The reconstructed pH
819 gradient remains broadly within the range of the modern values (0.19 to 0.3) although
820 there is some evidence of multi-million year scale variability.

821 As a caveat to our usage of the ΔpH -to- $\Delta\delta^{13}\text{C}$ relationship we point to changes of that
822 relationship that arise in our GENIE sensitivity experiments where carbon and
823 alkalinity inventories are manipulated, which can yield values outside of what is
824 plausible. We note that our CYCLOPS ensemble samples a very much wider range of
825 carbon and alkalinity inventories with $\Delta\text{pH}/\Delta\delta^{13}\text{C}$ remaining inside that range. While
826 CYCLOPS simulates the balance between weathering and CaCO_3 burial, which is
827 known to neutralize sudden carbon or alkalinity perturbations on timescales much
828 less than one million years, the configuration used for our GENIE simulations does
829 not and is therefore subject to states of ocean carbon chemistry that can safely be
830 ruled out for our study interval and likely for most of the Phanerozoic. The differing
831 outputs from CYCLOPS and GENIE in the DIC and ALK experiments does highlight
832 that $\Delta\text{pH}/\Delta\delta^{13}\text{C}$ actually depends on background seawater acid/base chemistry, in
833 ways that are not yet fully understood. That said, the generally coherent nature of our
834 results confirms we likely constrain the plausible range of $\Delta\text{pH}/\Delta\delta^{13}\text{C}$ for at least the
835 Neogene, if not the entire Cenozoic, outside of extreme events such as the
836 Palaeocene-Eocene Thermal Maximum.

837

838 3.3 $\delta^{11}\text{B}_{\text{sw}}$ record through the Neogene

839 Using input parameter uncertainties as described in section 2.5 yields individual
840 Monte Carlo member $\delta^{11}\text{B}_{\text{sw}}$ estimates between 30 ‰ and 43.5 ‰ at the overall
841 extreme points and typically ranging by ~10 ‰ (dashed in Fig. 10a) for each time
842 point, suggesting that the uncertainties we assign to the various input parameters are
843 generous enough not to predetermine the quantitative outcomes. However, for each

r.greenop 15/7/2016 16:15

Moved (insertion) [1]

r.greenop 15/7/2016 16:15

Deleted: The slope of the pH- $\delta^{13}\text{C}$ relationship simulated by our CYCLOPS model ensemble across a range of perturbed states is 0.2047 ($1\sigma = 0.0196$) (Fig. 7a, 8), in perfect agreement with modern empirical data and our GENIE experiments. Varying the biogeochemical parameters (gas exchange, rain ratio and remineralizing depth scale) yields some change in the regressed slope of the pH/ $\delta^{13}\text{C}$ relationship due to decoupled responses of pH and $\delta^{13}\text{C}$, but this gradient remains well within the 0.2 ± 0.05 range, and a RMSE of 0.05 in the spatial relationship remains robust (Fig. 6). We take this as evidence that the uncertainty in the pH/ $\delta^{13}\text{C}$ relationship assumed in our carbon chemistry calculation is well represented by a central value of 0.2 with a 0.025 standard deviation. Experiments at very high DIC or low alkalinity, either of which yield high atmospheric pCO_2 and low mean ocean pH, yield gradients slightly outside the 0.2 ± 0.05 range, with an elevated RMSE. This is probably associated with the non-linearity of the pH scale, modifying the gradient for a very different pH. It is to be emphasised that such extreme decoupled changes in DIC and alkalinity are not plausible within the Cenozoic, and were only possible in these simulations because of the absence of interactive sediments. . . [13]

r.greenop 15/7/2016 16:15

Moved up [1]: The slope of the pH- $\delta^{13}\text{C}$ relationship simulated by our CYCLOPS model ensemble across a range of perturbed states is 0.2047 ($1\sigma = 0.0196$) (Fig. 7a, 8), in perfect agreement with modern empirical data and our GENIE experiments.

r.greenop 18/7/2016 15:50

Deleted: s

r.greenop 18/7/2016 11:18

Deleted: The individual $\delta^{11}\text{B}_{\text{sw}}$ estimates calculated using the modern pH gradient method vary from 34.9 ‰ to 42.2 ‰ (± 0.84 -4.77 ‰) across the Neogene with a predominance of higher values closer to the modern and lowest values in the middle Miocene (Fig. 9). After smoothing is applied to satisfy seawater B mass balance, the long-term $\delta^{11}\text{B}_{\text{sw}}$ is determined as 37.5 ‰ at 23 Ma, decreases to a minimum of 37.17 ‰ a . . [14]

r.greenop 18/7/2016 11:18

Moved down [2]: The variability in the estimations of $\delta^{11}\text{B}_{\text{sw}}$ for each individual benthic/planktonic foraminifera pair suggest that individual estimates of $\delta^{11}\text{B}_{\text{sw}}$ are sensitive to the different input parameters, particularly the assigned uncertainty in the pH gradient. However, by smoothing the record we effectively suppress error that is uncorrelated between individual benthic/planktonic p . . [15]

939 planktic/benthic time point most individual Monte Carlo $\delta^{11}\text{B}_{\text{sw}}$ estimates fall into a
940 much narrower central range (~1 ‰ to 4 ‰; thick black line showing interquartile
941 range in Fig. 10a). The $\delta^{11}\text{B}_{\text{sw}}$ for Plio-Pleistocene time-points cluster around ~40 ‰
942 while middle/late Miocene values cluster around ~36.5 ‰. The estimates at
943 individual time points are completely independent from each other, such that the
944 observed clustering is strong evidence for an underlying long-term signal in our data,
945 albeit one that is obscured by the uncertainties involved in our individual $\delta^{11}\text{B}_{\text{sw}}$
946 estimates. The same long-term signal is also evident when pooling the individual
947 Monte Carlo member $\delta^{11}\text{B}_{\text{sw}}$ estimates into 8 million year bins and evaluating the
948 mean and spread (2σ) in each bin (Fig. 10b). This simple treatment highlights that
949 there is a significant difference between our Plio-Pleistocene and middle Miocene
950 data bins at the 95% confidence level and that $\delta^{11}\text{B}_{\text{sw}}$ appears to also have been
951 significantly lower than modern during the early Miocene.

952 3.3.1 Data smoothing

953 The ~1 to 4 ‰ likely ranges for $\delta^{11}\text{B}_{\text{sw}}$ would seem to be rather disappointing given
954 the goal to constrain $\delta^{11}\text{B}_{\text{sw}}$ for pH reconstructions. However, most of that uncertainty
955 is stochastic, random error that is uncorrelated from time point to time point.
956 Furthermore, we know from mass balance considerations that $\delta^{11}\text{B}_{\text{sw}}$ of seawater
957 should not change by more than ~0.1 ‰ per million years (Lemarchand et al., 2000)
958 and we use this as an additional constraint via the LOWESS smoothing we apply to
959 each Monte Carlo time series. One consideration is that each and every individual
960 Monte Carlo $\delta^{11}\text{B}_{\text{sw}}$ estimate is equally likely and the smoothing should therefore
961 target randomly selected individual Monte Carlo $\delta^{11}\text{B}_{\text{sw}}$ estimates, as we do here,
962 rather than smoothing over the likely ranges identified for each time point. In this
963 way the smoothing becomes integral part of our Monte Carlo uncertainty propagation
964 and the spread among the 10,000 individual smoothed $\delta^{11}\text{B}_{\text{sw}}$ curves carries the full
965 representation of propagated input uncertainty conditional on the boron cycle mass
966 balance constraint. A second consideration is that the smoothing should only remove
967 noise, not underlying signal. As detailed above, for this reason the smoothing
968 parameter we choose has enough freedom to allow the $\delta^{11}\text{B}_{\text{sw}}$ change to be dictated
969 by the data, with only the most extreme shifts in $\delta^{11}\text{B}_{\text{sw}}$ removed. We also tested the
970 robustness of the smoothing procedure itself (not shown) and found only marginal
971 changes when changing algorithm (LOESS versus LOWESS, with and without

r.greenop 18/7/2016 11:24

Deleted: When using $\delta^{13}\text{C}$ gradients as predictors for the pH gradient the $\delta^{11}\text{B}_{\text{sw}}$ values calculated are broadly similar to the results with assumed constant pH gradient: $\delta^{11}\text{B}_{\text{sw}}$ varies from 34.1 ‰ to 42.3 ‰ (± 0.72 -4.0 ‰) across the Neogene with the predominance of higher values closer to the modern with the lowest values in the middle Miocene (Fig. 9). However, when the individual $\delta^{11}\text{B}_{\text{sw}}$ estimates are smoothed, while the $\delta^{11}\text{B}_{\text{sw}}$ calculated using this method is similar to the constant pH gradient scenario through the late and middle Miocene (~ 37.5 ‰ ± 0.19 -1.28 ‰), the subsequent increase occurs more rapidly and the $\delta^{11}\text{B}_{\text{sw}}$ record reaches modern values by ~5 Ma (Fig. 9). The variability in the estimations of $\delta^{11}\text{B}_{\text{sw}}$ for each individual benthic/planktic foraminifera pair suggest that individual estimates of $\delta^{11}\text{B}_{\text{sw}}$ are sensitive to the different input parameters, particularly the assigned uncertainty in the pH gradient. However, by smoothing the record we effectively suppress error that is uncorrelated between individual benthic/planktic pairs of similar age and thereby focus on the effect of changes in $\delta^{11}\text{B}_{\text{sw}}$ that are correlated over multi-million year timescales. ... [16]

r.greenop 18/7/2016 11:18

Moved (insertion) [2]

1000 robust option) or when reducing the amount of smoothing (i.e., increasing the
1001 allowed rate $\delta^{11}\text{B}_{\text{sw}}$ change). The robustness of our smoothing is further underscored
1002 by the good correspondence with the results of simple data binning (Fig.10b).

1003

1004 **3.4 Comparison to other $\delta^{11}\text{B}_{\text{sw}}$ records**

1005 The comparison of our new $\delta^{11}\text{B}_{\text{sw}}$ record to those previously published reveals that
1006 despite the differences in methodology the general trends in the records show
1007 excellent agreement. The most dominant common feature of all the existing estimates
1008 of Neogene $\delta^{11}\text{B}_{\text{sw}}$ evolution is an increase through time from the middle Miocene to
1009 the Plio-Pleistocene (Fig. 11). While the model-based $\delta^{11}\text{B}_{\text{sw}}$ record of Lemarchand et
1010 al. (2000) is defined by a monotonous and very steady rise over the entire study
1011 interval, all three measurement-based records, including our own, are characterized
1012 by a single dominant phase of increase between roughly 12 and 5 Ma. Strikingly, the
1013 Pearson and Palmer (2000) record falls almost entirely within our 95% likelihood
1014 envelope, overall displaying very similar patterns of long-term change but with a
1015 relatively muted amplitude and overall rate of change relative to our reconstruction.
1016 Conversely, some of the second-order variations in the reconstruction by Raitzsch
1017 and Hönisch (2013) are not well matched by our reconstruction, but the dominant
1018 episode of rapid $\delta^{11}\text{B}_{\text{sw}}$ rise following the middle Miocene is in almost perfect
1019 agreement. We are encouraged by these agreements resulting from approaches based
1020 on very different underlying assumptions and techniques, which we take as indication
1021 for an emerging consensus view of $\delta^{11}\text{B}_{\text{sw}}$ evolution over the last 25 Ma and as a
1022 pathway towards reconstructing $\delta^{11}\text{B}_{\text{sw}}$ further back in time. Below we discuss in
1023 more detail the remaining discrepancies between our new and previously existing
1024 $\delta^{11}\text{B}_{\text{sw}}$ reconstructions.

1025 The record by Pearson and Palmer (2000) is well correlated to our reconstruction, but
1026 especially during the early Miocene there is a notable $\sim 0.5 \text{‰}$ offset (Fig. 11). This
1027 discrepancy could be due to a number of factors. Firstly, the applicability of this
1028 $\delta^{11}\text{B}_{\text{sw}}$ -record (derived from $\delta^{11}\text{B}$ data measured using NTIMS) to $\delta^{11}\text{B}$ records
1029 generated using the MC-ICPMS is uncertain (Foster et al., 2013). In addition, this
1030 $\delta^{11}\text{B}_{\text{sw}}$ -record is determined using a fractionation factor of 1.0194 (Kakihana et al.,

r.greenop 17/8/2016 18:02

Deleted: ,

r.greenop 12/8/2016 12:17

Deleted: that a

r.greenop 12/8/2016 12:17

Deleted: present

r.greenop 21/7/2016 10:10

Deleted: 0

r.greenop 12/8/2016 12:18

Deleted:

r.greenop 12/8/2016 12:18

Deleted: Our new $\delta^{11}\text{B}_{\text{sw}}$ record is broadly similar to previously published estimates calculated using pH gradients in the surface ocean, in terms of both shape of the record and magnitude of the reconstructed changes, with the notable exception in the early and middle Miocene where $\delta^{11}\text{B}_{\text{sw}}$ in our record is 0.5 ‰ lower (Fig. 10) than the published estimates of Pearson and Palmer (2000). Unfortunately

r.greenop 18/7/2016 12:14

Moved (insertion) [3]

r.greenop 18/7/2016 15:09

Deleted: ,

1046 1977), whereas recent experimental data have shown the value to be higher (1.0272 ±
1047 0.0006, Klochko et al., 2006), although foraminiferal vital effects are likely to mute
1048 this discrepancy. Thirdly, given our understanding of the δ¹¹B difference between
1049 species/size fractions (Foster, 2008; Henehan et al., 2013), the mixed species and size
1050 fractions used to make the δ¹¹B measurements in that study may have introduced
1051 some additional uncertainty in the reconstructed δ¹¹B_{sw}. Conversely, there is
1052 substantial spread between our three time points during the earliest Miocene, which
1053 combined with the edge effect of the smoothing gives rise to a widening uncertainty
1054 envelope during the time of greatest disagreement with Pearson and Palmer (2000).
1055 This could be taken as indication that our reconstruction, rather than that of Pearson
1056 and Palmer, is biased during the early Miocene.

1057

1058 The δ¹¹B_{sw} record calculated using benthic δ¹¹B and assumed deep ocean pH changes
1059 (Raitzsch and Höönsch, 2013) is also rather similar to our δ¹¹B_{sw} reconstruction. The
1060 discrepancy between the two records in the early Miocene could plausibly be
1061 explained by bias in our record (see above) or may in part be as a result of the
1062 treatment of surface water pH in the study of Raitzsch and Höönsch (2013) and their
1063 assumption of constant surface-deep pH gradient (see Fig 9). The combined output
1064 from two carbon cycle box models is used to make the assumption that surface ocean
1065 pH near-linearly increased by 0.39 over the last 50 Myrs. The first source of surface
1066 water pH estimates is from the study of Ridgwell et al. (2005), where CO₂ proxy data
1067 including some derived using the boron isotope-pH proxy is used, leading to some
1068 circularity in the methodology. The second source of surface water pH estimates is
1069 from Tyrrell & Zeebe (2004) and based on GEOCARB where the circularity problem
1070 does not apply. While this linear pH increase broadly matches the CO₂ decline from
1071 proxy records between the middle Miocene and present, it is at odds with the CO₂
1072 proxy data during the early Miocene that show CO₂ was lower than the middle
1073 Miocene during this interval (Beerling and Royer, 2011). Consequently the proxy
1074 CO₂ and surface water pH estimates are not well described by the linear change in pH
1075 applied by Raitzsch and Höönsch (2013) across this interval, potentially contributing
1076 to the discrepancy between our respective δ¹¹B_{sw} reconstructions..

1077 Our new δ¹¹B_{sw} record falls within the broad uncertainty envelope of boron mass

r.greenop 17/8/2016 18:04

Deleted: the

r.greenop 17/8/2016 18:05

Deleted: values

r.greenop 17/8/2016 18:05

Deleted: ed

r.greenop 17/8/2016 18:05

Deleted: here, with 9 out of 16 of their individual samples falling inside our 95% confidence band even before considering the large individual sample uncertainties reported by Raitzsch and Höönsch (2013).

r.greenop 18/7/2016 15:02

Deleted: That said, the polynomial fit to the data applied by Raitzsch and Höönsch (2013) takes no account of the uncertainties of individual data points and produces an oscillating pattern that is inconsistent with our new reconstruction (Fig. 10). Furthermore, our

1092 balance calculations of Lemarchand et al. (2000), but those modelled values do not
1093 show the same level of multi-million year variability of either Raitzsch and Höönsch
1094 (2013) or our new record, therefore suggesting that the model does not fully account
1095 for aspects of the changes in the ocean inputs and outputs of boron through time on
1096 timescales less than ~10 million years.

r.greenop 26/7/2016 19:38

Deleted: 2

1097 In line with the conclusions of previous studies (e.g., Raitzsch and Höönsch, 2013),
1098 our data show that the $\delta^{11}\text{B}_{\text{sw}}$ signal in the fluid inclusions (Paris et al., 2010) is
1099 mostly likely a combination of the $\delta^{11}\text{B}_{\text{sw}}$ and some other factor such as a poorly
1100 constrained fractionation factor between the seawater and the halite. Brine-halite
1101 fractionation offsets of -20‰ to -30‰ and -5‰ are reported from laboratory and
1102 natural environments (Vengosh et al., 1992; Liu et al., 2000). These fractionations
1103 and riverine input during basin isolation will drive the evaporite-hosted boron to low-
1104 $\delta^{11}\text{B}$ isotope values such that the fluid inclusion record likely provides a lower limit
1105 for the $\delta^{11}\text{B}_{\text{sw}}$ through time (i.e. $\delta^{11}\text{B}_{\text{sw}}$ is heavier than the halite fluid inclusions of
1106 Paris et al. (2010)). In order for this halite record to be interpreted directly as $\delta^{11}\text{B}_{\text{sw}}$,
1107 a better understanding of the factor(s) controlling the fractionation during halite
1108 formation and any appropriate correction need to be better constrained.

r.greenop 5/9/2016 16:07

Deleted: some of the controls on ocean
inputs and outputs of boron are not fully
understood.

1109

1110 3.5 Common controls on the seawater isotopic ratios of B, Mg, Ca and Li

1111 Our new record of $\delta^{11}\text{B}_{\text{sw}}$ has some substantial similarities to secular change seen in
1112 other marine stable isotope records (Fig. 12). The lithium isotopic composition of
1113 seawater ($\delta^7\text{Li}_{\text{sw}}$) Misra and Froelich, 2012) and the calcium isotopic composition of
1114 seawater ($\delta^{44/40}\text{Ca}_{\text{sw}}$) Griffith et al., 2008) both increase through the Neogene, whereas
1115 the magnesium isotopic composition of seawater ($\delta^{26}\text{Mg}_{\text{sw}}$) decreases (Pogge von
1116 Strandmann et al., 2014) suggesting a similar control on the isotopic composition of
1117 all four elements across this time interval (Fig. 12). To further evaluate the
1118 correlation between these other marine isotope records and $\delta^{11}\text{B}_{\text{sw}}$, we interpolate and
1119 cross-plot $\delta^{11}\text{B}_{\text{sw}}$ and the $\delta^7\text{Li}_{\text{sw}}$, $\delta^{44/40}\text{Ca}_{\text{sw}}$ and $\delta^{26}\text{Mg}_{\text{sw}}$ records. This analysis suggests
1120 that the isotopic composition of $\delta^{11}\text{B}_{\text{sw}}$, $\delta^7\text{Li}_{\text{sw}}$, $\delta^{26}\text{Mg}_{\text{sw}}$ and $\delta^{44/40}\text{Ca}_{\text{sw}}$ are well
1121 correlated through the Neogene, although there is some scatter in these relationships

r.greenop 21/7/2016 10:10

Deleted: 1

r.greenop 5/9/2016 16:21

Deleted: (

r.greenop 5/9/2016 16:21

Deleted: (

r.greenop 21/7/2016 10:10

Deleted: 1

1130 (Fig. 13). Although the Sr isotope record shows a similar increase during the
1131 Neogene (Hodell et al., 1991), we focus our discussion on $\delta^{11}\text{B}_{\text{sw}}$, $\delta^7\text{Li}_{\text{sw}}$, $\delta^{26}\text{Mg}_{\text{sw}}$ and
1132 $\delta^{44/40}\text{Ca}_{\text{sw}}$ given that the factors fractionating these stable isotopic systems are similar
1133 (see below).

r.greenop 21/7/2016 10:10
Deleted: 2
r.greenop 5/9/2016 17:00
Deleted: elect to
r.greenop 5/9/2016 16:22
Deleted: e

1134 To better constrain the controls on $\delta^{11}\text{B}_{\text{sw}}$, $\delta^7\text{Li}_{\text{sw}}$, $\delta^{26}\text{Mg}_{\text{sw}}$ and $\delta^{44/40}\text{Ca}_{\text{sw}}$ it is
1135 instructive to compare the size and isotopic composition of the fluxes of boron,
1136 lithium, calcium and magnesium to the ocean (Table 3). The major flux of boron into
1137 the ocean is via riverine input (Lemarchand et al., 2000), although some studies
1138 suggest that atmospheric input may also play an important role (Park and
1139 Schlesinger, 2002). The loss terms are dominated by adsorption onto clays and the
1140 alteration of oceanic crust (Spivack and Edmond, 1987; Smith et al., 1995).

r.greenop 21/7/2016 11:48
Deleted: 1
r.greenop 5/9/2016 17:00
Deleted: As noted previously, t
r.greenop 26/7/2016 19:38
Deleted: 2
r.greenop 12/8/2016 12:21
Deleted: outputs
r.greenop 5/9/2016 17:00
Deleted: to boron

1141 Similarly, the primary inputs of lithium into the ocean come from hydrothermal
1142 sources and riverine input and the main outputs are ocean crust alteration and
1143 adsorption onto sediments (Misra and Froelich, 2012). The two dominant controls on
1144 magnesium concentration and isotope ratio in the oceans is the riverine input, ocean
1145 crust alteration and dolomitization (Table 3) (Tipper et al., 2006b). The main controls
1146 on the amount of calcium in the modern ocean and its isotopic composition is the
1147 balance between riverine and hydrothermal inputs and removal through CaCO_3
1148 deposition and alteration of oceanic crust (Fantle and Tipper, 2014, Griffith et al.,
1149 2008). Dolomitization has also been cited as playing a potential role in controlling
1150 $\delta^{44/40}\text{Ca}_{\text{sw}}$, although the contribution of this process through time is poorly constrained
1151 (Griffith et al., 2008).

r.greenop 21/7/2016 11:48
Deleted: 1

1152 Analysis of the oceanic fluxes of all four ions suggests that riverine input may be an
1153 important factor influencing the changing isotopic composition of B, Li, Ca and Mg
1154 over the late Neogene (Table 3). In the case of all four elements, a combination of the
1155 isotopic ratio of the source rock and isotopic fractionation during weathering
1156 processes are typically invoked to explain the isotopic composition of a particular
1157 river system. However, in most cases the isotopic composition of the source rock is
1158 found to be of secondary importance (Rose et al., 2000; Kisakürek et al., 2005;
1159 Tipper et al., 2006b; Millot et al., 2010). For instance, the $\delta^{11}\text{B}$ composition of rivers
1160 is primarily dependent on isotopic fractionation during the reaction of water with
1161 silicate rocks and to a lesser extent the isotopic composition of the source rock (i.e.

r.greenop 21/7/2016 11:48
Deleted: 1
r.greenop 5/9/2016 17:01
Deleted: used

1173 the proportion of evaporites and silicate rocks; Rose et al., 2000). While some studies
1174 have suggested that the isotopic composition of rainfall within the catchment area
1175 may be an important factor controlling the $\delta^{11}\text{B}$ in rivers (Rose-Koga et al., 2006),
1176 other studies have shown atmospheric boron to be a secondary control on riverine
1177 boron isotope composition (Lemarchand and Gaillardet, 2006). The source rock also
1178 appears to have limited influence on the $\delta^7\text{Li}$ composition of rivers and riverine $\delta^7\text{Li}$
1179 varies primarily with weathering intensity (Kisakürek et al., 2005; Millot et al.,
1180 2010). The riverine input of calcium to the oceans is controlled by the composition of
1181 the primary continental crust (dominated by carbonate weathering) and a recycled
1182 component, although the relative influence of these two processes is not well
1183 understood (Tipper et al., 2006a). In addition, vegetation may also play a significant
1184 role in the $\delta^{44/40}\text{Ca}$ of rivers (Fantle and Tipper, 2014). For Mg, the isotopic
1185 composition of the source rock is important for small rivers, however, lithology is of
1186 limited significance at a global scale in comparison to fractionation in the weathering
1187 environment (Tipper et al., 2006b). Given the lack of evidence of source rock as a
1188 dominant control on the isotopic composition of rivers, here we focus on some of the
1189 possible causes for changes in the isotopic composition and/or flux of riverine input
1190 over the Neogene.

1191 In this regard, of the four elements discussed here, the Li isotopic system is the most
1192 extensively studied. Indeed, the change in $\delta^7\text{Li}_{\text{sw}}$ has already been attributed to an
1193 increase in the $\delta^7\text{Li}_{\text{sw}}$ composition of the riverine input (Hathorne and James, 2006;
1194 Misra and Froelich, 2012). The causes of the shift in $\delta^7\text{Li}$ riverine have been variably
1195 attributed to: (1) an increase in incongruent weathering of silicate rocks and
1196 secondary clay formation as a consequence of Himalayan uplift (Misra and Froelich,
1197 2012), (2) a reduction in weathering intensity (Hathorne and James, 2006; Froelich
1198 and Misra, 2014), (3) an increase in silicate weathering rate (Liu et al., 2015) and 4)
1199 an increase in the formation of floodplains and the increased formation of secondary
1200 minerals (Pogge von Strandmann and Henderson, 2014). In all four cases the lighter
1201 isotope of Li is retained on land in clay and secondary minerals. A mechanism
1202 associated with either an increase in secondary mineral formation or the retention of
1203 these minerals on land is also consistent across Mg, Ca and B isotope systems. For
1204 instance, clay minerals are preferentially enriched in the light isotope of B (Spivack
1205 and Edmond, 1987; Deyhle and Kopf, 2004; Lemarchand and Gaillardet, 2006) and

1206 Li (Pistiner and Henderson, 2003) and soil carbonates and clays are preferentially
1207 enriched in the light isotope of Ca (Tipper et al., 2006a; Hindshaw et al., 2013;
1208 Ockert et al., 2013). The formation of secondary silicate minerals, such as clays, is
1209 assumed to preferentially take up the heavy Mg isotope into the solid phase (Tipper et
1210 al., 2006a; Tipper et al., 2006b; Pogge von Strandmann et al., 2008; Wimpenny et al.,
1211 2014), adequately explaining the inverse relationship between $\delta^{11}\text{B}_{\text{sw}}$ and $\delta^{26}\text{Mg}_{\text{sw}}$.
1212 Consequently the increased formation or retention on land of secondary minerals
1213 would alter the isotopic composition of the riverine input to the ocean in the correct
1214 direction to explain the trends in all four isotope systems through the late Neogene
1215 (Fig. 13). The increased formation and retention of clays on land may have been
1216 related to the growth of the Himalayan orogeny and increased clay formation in the
1217 newly formed floodplains and foreland surrounding the mountains (Pogge von
1218 Strandmann and Henderson, 2014).

r.greenop 12/8/2016 12:22
Deleted: of all the examined isotope systems and could potentially
r.greenop 21/7/2016 10:10
Deleted: 2

r.greenop 12/8/2016 12:30
Formatted: Font color: Auto, English (UK)

1219 4 Conclusions

1220 Here we present a new $\delta^{11}\text{B}_{\text{sw}}$ record for the Neogene based on paired planktic-
1221 benthic $\delta^{11}\text{B}$ measurements. Our new record suggests that $\delta^{11}\text{B}_{\text{sw}}$ (i) was ~ 37.5 ‰ at
1222 the Oligocene-Miocene boundary, (ii) remained low through the middle Miocene,
1223 (iii) rapidly increased to the modern value between 12 and 5 Ma, and (iv) plateaued at
1224 modern values over the Plio-Pleistocene. Despite some disagreements, the fact that
1225 our new record, and both of the published data based reconstructions capture the first-
1226 order late Miocene $\delta^{11}\text{B}_{\text{sw}}$ rise suggests that consensus is building for the $\delta^{11}\text{B}_{\text{sw}}$
1227 evolution through the Neogene. This emerging view on $\delta^{11}\text{B}_{\text{sw}}$ change provides a vital
1228 constraint required to quantitatively reconstruct Neogene ocean pH, ocean carbon
1229 chemistry and atmospheric CO₂ using the $\delta^{11}\text{B}$ -pH proxy. When our new $\delta^{11}\text{B}_{\text{sw}}$
1230 record is compared to changes in the seawater isotopic composition of Li, Ca and Mg
1231 the shape of the records across the Neogene is remarkably similar. In all four cases
1232 riverine input is cited as one of the key control of the isotopic composition of the
1233 elements in seawater. When we compare the isotopic fractionation of the elements
1234 associated with secondary mineral formation, the trends in the $\delta^{26}\text{Mg}_{\text{sw}}$, $\delta^{44/40}\text{Ca}_{\text{sw}}$
1235 $\delta^{11}\text{B}_{\text{sw}}$ and $\delta^7\text{Li}_{\text{sw}}$ records are all consistent with an increase in secondary mineral
1236 formation through time. While a more quantitative treatment of these multiple stable

r.greenop 12/8/2016 12:22
Deleted: is
r.greenop 12/8/2016 12:23
Deleted: and
r.greenop 12/8/2016 12:26
Deleted: s

r.greenop 12/8/2016 12:26
Deleted: . $\delta^{11}\text{B}_{\text{sw}}$ then increases to the modern value through the late Miocene. This new $\delta^{11}\text{B}_{\text{sw}}$ record provides a vital constraint required to estimate Neogene ocean pH, ocean carbon chemistry and atmospheric CO₂ using the $\delta^{11}\text{B}$ -pH proxy.

r.greenop 5/9/2016 16:23
Deleted: the

1250 isotope systems is required, the $\delta^{11}\text{B}_{\text{sw}}$ record presented here provides additional
1251 constraints on the processes responsible for the evolution of ocean chemistry through
1252 time.

1253 **Acknowledgements:**

1254 This work used samples provided by (I)ODP, which is sponsored by the U.S.
1255 National Science Foundation and participating countries under the management of
1256 Joint Oceanographic Institutions, Inc. We thank W. Hale and A. Wuelbers of the
1257 Bremen Core Repository for their kind assistance. The work was supported by NERC
1258 grants NE/I006176/1 (G.L.F. and C.H.L.), NE/H006273/1 (G.L.F), NE/I006168/1
1259 and NE/K014137/1 [and a Royal Society Research Merit Award](#) (P.A.W), a NERC
1260 Independent Research Fellowship NE/K00901X/1 (M.P.H.) and a NERC studentship
1261 (R.G). Matthew Cooper, J. Andy Milton, and the B-team are acknowledged for their
1262 assistance in the laboratory.

1263

1264

1265 **References:**

- 1266 Al-Rousan, S., Pätzold, J., Al-Moghrabi, S., and Wefer, G., 2004, Invasion of
1267 anthropogenic CO₂ recorded in planktonic foraminifera from the northern Gulf
1268 of Aqaba: International Journal of Earth Sciences, v. 93, no. 6, p. 1066-1076.
1269 [Anagnostou, E., John, E.H., Edgar, K.M., Foster, G.L., Ridgewell, A., Inglis, G.N.,](#)
1270 [Pancost, R.D., Lunt, D.J., Pearson, P.N., 2016, Changing atmospheric CO₂](#)
1271 [concentration was the primary driver of early Cenozoic climate, v. 533, p. 380-](#)
1272 [384.](#)
- 1273 Anand, P., Elderfield, H., and Conte, M. H., 2003, Calibration of Mg/Ca
1274 thermometry in planktonic foraminifera from a sediment trap time series:
1275 Paleoceanography, v. 18, no. 2, DOI: 10.1029/2002PA000846.
- 1276 Bartoli, G., Höönsch, B., Zeebe, R.E., 2011, Atmospheric CO₂ decline during the
1277 Pliocene intensification of Northern Hemisphere glaciations:
1278 Paleoceanography, v.26, DOI: 10.1029/2010PA002055.
- 1279 Badger, M. P. S., Lear, C.H., Pancost, R.D., Foster, G.L., Bailey, T.R., Leng, M.J.,
1280 and Abels, H.A., 2013, CO₂ drawdown following the middle Miocene
1281 expansion of the Antarctic Ice Sheet: Paleoceanography, v. 28,
1282 doi:10.1002/palo.20015.
- 1283 Beerling, D. J., and Royer, D. L., 2011, Convergent Cenozoic CO₂ history: Nature
1284 Geosci, v. 4, no. 7, p. 418-420.

- 1285 Berner, R. A., and Kothavala, Z., 2001, GEOCARB III: A revised model of
1286 atmospheric CO₂ over Phanerozoic time: American Journal of Science, v. 301,
1287 no. 2, p. 182-204.
- 1288 Brennan S. T., Lowenstein T. K., Cendón D. I., 2013, The major-ion composition of
1289 Cenozoic seawater: the past 36 million years from fluid inclusions in marine
1290 halite: American Journal of Science, v. 313, p. 713–775.
- 1291 Broecker, W. S. and T. H. Peng, 1982, Tracers in the Sea, Lamont-Doherty Earth
1292 Observatory, Palisades, N. Y.
- 1293 Burton, K.W., Vigier, N., 2012, Lithium isotopes as tracers in Marine and terrestrial
1294 environments, Handbook of Environmental Isotope Geochemistry, Springer,
1295 Berlin, Heidelberg, p. 41–59.
- 1296 CARINA Group, 2009, Carbon in the Atlantic Ocean Region - the CARINA project:
1297 Results and Data, Version 1.0: Carbon Dioxide Information Analysis Center,
1298 Oak Ridge National Laboratory, U.S. Department of Energy, Oak Ridge,
1299 Tennessee. doi: 10.3334/CDIAC/otg.CARINA.ATL.V1.0
- 1300 Catanzaro, E. J., Champion, C., Garner, E., Marinenco, G., Sappenfield, K., and W.,
1301 S., 1970, Boric Acid: Isotopic and Assay Standard Reference Materials NBS
1302 (US) Special Publications. National Bureau of Standards, Institute for
1303 Materials Research, Washington, DC.
- 1304 Cramer, B., Miller, K., Barrett, P., and Wright, J., 2011, Late Cretaceous-Neogene
1305 trends in deep ocean temperature and continental ice volume: Reconciling
1306 records of benthic foraminiferal geochemistry ($\delta^{18}\text{O}$ and Mg/Ca) with sea
1307 level history: Journal of Geophysical Research-Oceans, v. 116,
1308 doi:10.1029/2011JC007255.
- 1309 Delaney, M. L., Be, A. W. H., and Boyle, E. A., 1985, Li, Sr, Mg and Na in
1310 foraminiferal calcite shells from laboratory culture, sediment traps and
1311 sediment cores: Geochimica Et Cosmochimica Acta, v. 49, no. 6, p. 1327-
1312 1341.
- 1313 Deyhle, A., and Kopf, A., 2004, Possible influence of clay contamination on B
1314 isotope geochemistry of carbonaceous samples: Applied Geochemistry, v. 19,
1315 no. 5, p. 737-745.
- 1316 Edwards, N. R. and Marsh, R., 2005, Uncertainties due to transport- parameter
1317 sensitivity in an efficient 3-D ocean-climate model: Clim. Dynam., 24, 415-
1318 433, doi:10.1007/s00382-004-0508-8.
- 1319 Elderfield, H., Yu, J., Anand, P., Kiefer, T., and Nyland, B., 2006, Calibrations for
1320 benthic foraminiferal Mg/Ca paleothermometry and the carbonate ion
1321 hypothesis: Earth and Planetary Science Letters, v. 250, no. 3-4, p. 633-649.
- 1322 Evans, D., and Muller, W., 2012, Deep time foraminifera Mg/Ca paleothermometry:
1323 Nonlinear correction for secular change in seawater Mg/Ca:
1324 Paleoceanography, v. 27, DOI: 10.1029/2012PA002315.
- 1325 Fantle, M.S., Tipper, E.T., 2014, Calcium isotopes in the global biogeochemical Ca
1326 cycle: Implications for development of a Ca isotope proxy, Earth-Science
1327 Reviews, v. 129, p. 148-177.
- 1328 Foster, G., Höönsch, B., Paris, G., Dwyer, G., Rae, J., Elliott, T., Gaillardet, J.,
1329 Hemming, N., Louvat, P., and Vengosh, A., 2013, Interlaboratory comparison
1330 of boron isotope analyses of boric acid, seawater and marine CaCO₃ by MC-
1331 ICPMS and NTIMS: Chemical Geology, v. 358, p. 1-14.
- 1332 Foster, G., Lear, C. H., and Rae, J.W.B., 2012, The evolution of $p\text{CO}_2$, ice volume
1333 and climate during the middle Miocene: Earth and Planetary Science Letters,
1334 v. 341-344, p. 243-254.

- 1335 Foster, G. L., 2008, Seawater pH, $p\text{CO}_2$ and $[\text{CO}_3^{2-}]$ variations in the Caribbean Sea
1336 over the last 130 kyr: A boron isotope and B/Ca study of planktic foraminifera:
1337 *Earth and Planetary Science Letters*, v. 271, no. 1-4, p. 254-266.
- 1338 Foster, G. L., Pogge von Strandmann, P. A. E., and Rae, J. W. B., 2010, Boron and
1339 magnesium isotopic composition of seawater: *Geochemistry Geophysics
1340 Geosystems*, v. 11, DOI: 10.1029/2010GC003201.
- 1341 Froelich, F., and Misra, S., 2014. Was the late Paleocene-early Eocene hot because
1342 Earth was flat? An ocean lithium isotope view of mountain building,
1343 continental weathering, carbon dioxide, and Earth's Cenozoic climate:
1344 *Oceanography*, v. 27, no. 1, p. 36-49.
- 1345 Galbraith, E.D., Kwon, E.Y., Bianchi, D., Hain, M.P., Sarmiento, J.L., 2015, The
1346 impact of atmospheric $p\text{CO}_2$ on carbon isotope ratios of the atmosphere and
1347 ocean: *Global Biogeochemical Cycles*, 9, 307-324,
1348 doi:10.1002/2014GB004929
- 1349 Goodwin, P., and J. M. Lauderdale 2013, Carbonate ion concentrations, ocean carbon
1350 storage, and atmospheric CO₂: *Global Biogeochem. Cycles*, 27,
1351 doi:10.1002/gbc.20078.
- 1352 Gradstein F.M., Ogg J.G., Schmitz M., Ogg G., 2012, *The Geologic Time Scale
1353 2012*: Boston, Elsevier, 1144 p., doi:10.1016/B978-0-444-59425-9.00004-4.
- 1354 Greenop, R., Foster, G. L., Wilson, P. A., and Lear, C. H., 2014, Middle Miocene
1355 climate instability associated with high-amplitude CO₂ variability:
1356 *Paleoceanography*, v. 29, no. 9, DOI: 2014PA002653.
- 1357 Griffith, E., Paytan, A., Caldeira, K., Bullen, T., and Thomas, E., 2008, A Dynamic
1358 Marine Calcium Cycle During the Past 28 Million Years: *Science*, v. 322, no.
1359 5908, p. 1671-1674.
- 1360 Hain, M.P., Sigman, D.M., and Haug, G.H., 2010, Carbon dioxide effects of
1361 Antarctic stratification, North Atlantic Intermediate Water formation, and
1362 subantarctic nutrient drawdown during the last ice age: Diagnosis and
1363 synthesis in a geochemical box model: *Global Biogeochem. Cycles*, v. 24,
1364 doi:10.1029/2010GB003790.
- 1365 Hain, M.P., Sigman, D.M., and Haug, G.H., 2014a, The Biological Pump in the Past,
1366 *Treatise on Geochemistry 2nd ed.*, vol. 8, chapter 18, 485-517,
1367 doi:10.1016/B978-0-08-095975-7.00618-5
- 1368 Hain, M.P., Sigman, D.M., and Haug, G.H., 2014b, Distinct roles of the Southern
1369 Ocean and North Atlantic in the deglacial atmospheric radiocarbon decline:
1370 *Earth and Planetary Science Letters*, v.394, p.198-208, doi:
1371 10.1016/j.epsl.2014.03.020
- 1372 Hain, M.P., Sigman, D.M., Higgins, J.A., and Haug, G.H., 2015, The effects of
1373 secular calcium and magnesium concentration changes on the
1374 thermodynamics of seawater acid/base chemistry: Implications for Eocene
1375 and Cretaceous ocean carbon chemistry and buffering: *Global Biogeochem.
1376 Cycles*, v. 29, doi:10.1002/2014GB004986.
- 1377 Hasiuk, F., and Lohmann, K., 2010, Application of calcite Mg partitioning functions
1378 to the reconstruction of paleocean Mg/Ca: *Geochimica Et Cosmochimica
1379 Acta*, v. 74, no. 23, p. 6751-6763.
- 1380 Hathorne, E. C., and James, R. H., 2006, Temporal record of lithium in seawater: A
1381 tracer for silicate weathering?: *Earth and Planetary Science Letters*, v. 246,
1382 no. 3-4, p. 393-406.

- 1383 Haug, G. H., and Tiedemann, R., 1998, Effect of the formation of the Isthmus of
 1384 Panama on Atlantic Ocean thermohaline circulation: *Nature*, v. 393, no. 6686,
 1385 p. 673-676.
- 1386 Hemleben Ch, Spindler M, Breitinger, Ott R., 1987, Morphological and physiological
 1387 responses of *Globigerinoides sacculifer* (Brady) under varying laboratory
 1388 conditions: *Marine Micropaleontology*, v.12, p. 305-324.
- 1389 Hemming, N. G., and Hanson, G. N., 1992, Boron isotopic composition and
 1390 concentration in modern marine carbonates: *Geochimica et Cosmochimica
 1391 Acta*, v. 56, no. 1, p. 537-543.
- 1392 Henehan, M. J., Rae, J. W. B., Foster, G. L., Erez, J., Prentice, K. C., Kucera, M.,
 1393 Bostock, H. C., Martinez-Botí, M. A., Milton, J. A., Wilson, P. A., Marshall,
 1394 B. J., and Elliott, T., 2013, Calibration of the boron isotope proxy in the
 1395 planktonic foraminifera *Globigerinoides ruber* for use in palaeo-CO₂
 1396 reconstruction: *Earth and Planetary Science Letters*, v. 364, no. 0, p. 111-122.
- 1397 Hindshaw, R. S., Bourdon, B., Pogge von Strandmann, P. A. E., Vigier, N., and
 1398 Burton, K. W., 2013, The stable calcium isotopic composition of rivers
 1399 draining basaltic catchments in Iceland: *Earth and Planetary Science Letters*,
 1400 v. 374, no. 0, p. 173-184.
- 1401 Hodell, D.A., Mueller, P.A., Garrido, J.R., 1991, Variations in the strontium isotopic
 1402 composition of seawater during the Neogene: *Geology*, v.11, p. 24-27.
- 1403 Holbourn, A., Kuhnt, W., Simo, J., and Li, Q., 2004, Middle Miocene isotope
 1404 stratigraphy and paleceanographic evolution of the northwest and southwest
 1405 Australian margins (Wombat Plateau and Great Australian Bight):
 1406 *Palaeogeography Palaeoclimatology Palaeoecology*, v. 208, no. 1-2, p. 1-22.
- 1407 Holden, P. B., N. R. Edwards, S. A. Müller, K. I. C. Oliver, R. M. De'ath and A.
 1408 Ridgwell, 2013. Controls on the spatial distribution of oceanic $\delta^{13}\text{C}_{\text{DIC}}$:
 1409 *Biogeosciences* 10, 1815-1833.
- 1410 Höönsch, B., Hemming, N. G., Archer, D., Siddall, M., and McManus, J. F., 2009,
 1411 Atmospheric Carbon Dioxide Concentration Across the Mid-Pleistocene
 1412 Transition: *Science*, v. 324, no. 5934, p. 1551-1554.
- 1413 Horita, J., Zimmermann, H., and Holland, H. D., 2002, Chemical evolution of
 1414 seawater during the Phanerozoic: Implications from the record of marine
 1415 evaporites: *Geochimica Et Cosmochimica Acta*, v. 66, no. 21, p. 3733-3756.
- 1416 Kaczmarek, K., Nehrke, G., Misra, S., Bijma, J., Elderfield, H., 2016, Investigating
 1417 the effects of growth rate and temperature on the B/Ca ratio and $\delta^{11}\text{B}$ during
 1418 inorganic calcite formation, v. 421, p. 81-92.
- 1419 Kakihana, H., Kotaka, M., Satoh, S., Nomura, M., and Okamoto, M., 1977,
 1420 Fundamental studies on ion-exchange separation of boron isotopes: *Bulletin
 1421 of the Chemical Society of Japan*, v. 50, no. 1, p. 158-163.
- 1422 Keeling, C.D., 1979, The Suess effect: ¹³Carbon-¹⁴Carbon interrelations: Environment
 1423 International, v. 2, no. 4-6, p. 229-300.
- 1424 Key, R. M., Kozyr, A., Sabine, C. L., Lee, K., Wanninkhof, R., Bullister, J. L., Feely,
 1425 R. A., Millero, F. J., Mordy, C., and Peng, T. H., 2004, A global ocean carbon
 1426 climatology: Results from Global Data Analysis Project (GLODAP): *Global
 1427 Biogeochem. Cycles*, v. 18, no. 4, doi:10.1029/2004GB002247.
- 1428 Kisakürek, B., James, R. H., and Harris, N. B. W., 2005, Li and $\delta^7\text{Li}$ in Himalayan
 1429 rivers: Proxies for silicate weathering?: *Earth and Planetary Science Letters*,
 1430 v. 237, no. 3-4, p. 387-401.

- 1431 Klochko, K., Kaufman, A. J., Yao, W. S., Byrne, R. H., and Tossell, J. A., 2006,
 1432 Experimental measurement of boron isotope fractionation in seawater: Earth
 1433 and Planetary Science Letters, v. 248, no. 1-2, p. 276-285.
- 1434 Lear, C. H., Mawbey, E. M., and Rosenthal, Y., 2010, Cenozoic benthic foraminiferal
 1435 Mg/Ca and Li/Ca records: Toward unlocking temperatures and saturation
 1436 states: Paleoceanography, v. 25, doi:10.1029/2009PA001880.
- 1437 Lee, K., Kim, T. W., Byrne, R. H., Millero, F. J., Feely, R. A., and Liu, Y. M., 2010,
 1438 The universal ratio of boron to chlorinity for the North Pacific and North
 1439 Atlantic oceans: Geochimica Et Cosmochimica Acta, v. 74, no. 6, p. 1801-
 1440 1811.
- 1441 Lemarchand, D., and Gaillardet, J., 2006, Transient features of the erosion of shales
 1442 in the Mackenzie basin (Canada), evidences from boron isotopes: Earth and
 1443 Planetary Science Letters, v. 245, no. 1-2, p. 174-189.
- 1444 Lemarchand, D., Gaillardet, J., Lewin, E., and Allegre, C. J., 2000, The influence of
 1445 rivers on marine boron isotopes and implications for reconstructing past ocean
 1446 pH, Nature, v. 408, p. 951-954.
- 1447 Liu, W. G., Xiao, Y. K., Peng, Z. C., An, Z. S., and He, X. X., 2000, Boron
 1448 concentration and isotopic composition of halite from experiments and salt
 1449 lakes in the Qaidam Basin: Geochimica Et Cosmochimica Acta, v. 64, no. 13,
 1450 p. 2177-2183.
- 1451 Liu, X.-M., Wanner, C., Rudnick, R. L., and McDonough, W. F., 2015, Processes
 1452 controlling $\delta^7\text{Li}$ in rivers illuminated by study of streams and groundwaters
 1453 draining basalts: Earth and Planetary Science Letters, v. 409, no. 0, p. 212-
 1454 224.
- 1455 Lynch-Steiglitz, J., T.F. Stocker, W.S. Broecker and R.G. Fairbanks (1995), The
 1456 influence of air-sea exchange on the isotopic composition of oceanic carbon:
 1457 Observations and modeling: Global Biogeochemical Cycles, vol. 9, 4, p653-
 1458 665.
- 1459 Martínez-Botí, M. A., Foster, G. L., Chalk, T. B., Rohling, E. J., Sexton, P. F., Lunt,
 1460 D. J., Pancost, R. D., Badger, M. P. S., and Schmidt, D. N., 2015a, Plio-
 1461 Pleistocene climate sensitivity from on a new high-resolution CO₂ record:
 1462 Nature, v. 518, p. 49-54.
- 1463 Martínez-Botí, M.A., Marino, G., Foster, G. L., Ziveri, P., Henehan, M. J., Rae, J. W.
 1464 B., Mortyn, P. G. and Vance, D., 2015b, Boron isotope evidence for oceanic
 1465 CO₂ leakage during the last deglaciation: Nature, v. 518, p. 219-222.
- 1466 McCorkle, D. C., Corliss, B. H., and Farnham, C. A., 1997, Vertical distributions and
 1467 stable isotopic compositions of live (stained) benthic foraminifera from the
 1468 North Carolina and California continental margins: Deep Sea Research Part I:
 1469 Oceanographic Research Papers, v. 44, no. 6, p. 983-1024.
- 1470 Millot, R., Vigier, N., and Gaillardet, J., 2010, Behaviour of lithium and its isotopes
 1471 during weathering in the Mackenzie Basin, Canada: Geochimica et
 1472 Cosmochimica Acta, v. 74, no. 14, p. 3897-3912.
- 1473 Misra, S., and Froelich, P., 2012, Lithium Isotope History of Cenozoic Seawater:
 1474 Changes in Silicate Weathering and Reverse Weathering: Science, v. 335, no.
 1475 6070, p. 818-823.
- 1476 Ockert, C., Gussone, N., Kaufhold, S., Teichert, B.M.A., 2013, Isotope fractionation
 1477 during Ca exchange on clay minerals in a marine environment: Geochimica et
 1478 Cosmochimica Acta, v. 112, p. 374-388.
- 1479 Olsen, A., Ninneman, U.S., 2010, Large $\delta^{13}\text{C}$ gradients in the preindustrial North
 1480 Atlantic revealed: Science, v. 330, p. 658-659.

r.greenop 26/7/2016 19:35

Deleted: 2

r.greenop 26/7/2016 19:36

Formatted: Font:(Default) Times New Roman, 12 pt

r.greenop 26/7/2016 19:35

Deleted: Boron isotope systematics in large rivers: implications for the marine boron budget and paleo-pH reconstruction over the Cenozoic

r.greenop 26/7/2016 19:36

Deleted: Chemical Geology

r.greenop 26/7/2016 19:36

Deleted: 190

r.greenop 26/7/2016 19:36

Deleted: no. 1-4,

r.greenop 26/7/2016 19:36

Deleted: 123

r.greenop 26/7/2016 19:36

Deleted: 140

- 1491 Pälike, H., Lyle, M., Nishi, H., Raffi, I., Ridgwell, A., Gamage, K., Klaus, A., Acton,
1492 G., Anderson, L., Backman, J., Baldauf, J., Beltran, C., *et al.* 2012, A
1493 Cenozoic record of the equatorial Pacific carbonate compensation depth:
1494 Nature, v. 488, no. 7413, p. 609-614.
- 1495 Palmer, M. R., Pearson, P. N., and Cobb, S. J., 1998, Reconstructing past ocean pH-
1496 depth profiles: Science, v. 282, no. 5393, p. 1468-1471.
- 1497 Paris, G., Gaillardet, J., and Louvat, P., 2010, Geological evolution of seawater boron
1498 isotopic composition recorded in evaporites: Geology, v. 38, no. 11, p. 1035-
1499 1038.
- 1500 Park, H., and Schlesinger, W. H., 2002, Global biogeochemical cycle of boron:
1501 Global Biogeochemical Cycles, v. 16, no. 4, DOI: 10.1029/2001GB001766.
- 1502 Pearson, P. N., Foster, G. L., and Wade, B. S., 2009, Atmospheric carbon dioxide
1503 through the Eocene-Oligocene climate transition: Nature, v. 461, p. 1110-
1504 1113.
- 1505 Pearson, P. N., and Wade, B. S., 2009, Taxonomy and Stable Isotope Paleoecology of
1506 Well-Preserved Planktonic Foraminifera from the Uppermost Oligocene of
1507 Trinidad: Journal of Foraminiferal Research, v. 39, no. 3, p. 191-217.
- 1508 Pearson, P. N., and Palmer, M. R., 1999, Middle Eocene seawater pH and
1509 atmospheric carbon dioxide concentrations: Science, v. 284, no. 5421, p.
1510 1824-1826.
- 1511 Pearson, P. N., and Palmer, M. R., 2000, Atmospheric carbon dioxide concentrations
1512 over the past 60 million years: Nature, v. 406, no. 6797, p. 695-699.
- 1513 Pistiner, J. S., and Henderson, G. M., 2003, Lithium-isotope fractionation during
1514 continental weathering processes: Earth and Planetary Science Letters, v. 214,
1515 no. 1-2, p. 327-339.
- 1516 Pogge von Strandmann, P. A. E., Burton, K. W., James, R. H., van Calsteren, P.,
1517 Gislason, S. R., and Sigfusson, B., 2008, The influence of weathering
1518 processes on riverine magnesium isotopes in a basaltic terrain: Earth and
1519 Planetary Science Letters, v. 276, no. 1-2, p. 187-197.
- 1520 Pogge von Strandmann, P. A. E., Forshaw, J., and Schmidt, D. N., 2014, Modern and
1521 Cenozoic records of seawater magnesium from foraminiferal Mg isotopes:
1522 Biogeosciences, v. 11, no. 18, p. 5155-5168.
- 1523 Pogge von Strandmann, P. A. E., and Henderson, G. M., 2014, The Li isotope
1524 response to mountain uplift: Geology, doi: 10.1130/G36162.1.
- 1525 Rae, J. W. B., Foster, G. L., Schmidt, D. N., and Elliott, T., 2011, Boron isotopes and
1526 B/Ca in benthic foraminifera: Proxies for the deep ocean carbonate system:
1527 Earth and Planetary Science Letters, v. 302, no. 3-4, p. 403-413.
- 1528 Raitzsch, M., and Hönnisch, B., 2013, Cenozoic boron isotope variations in benthic
1529 foraminifers: Geology, v. 41, no. 5, p. 591-594.
- 1530 Ridgewell, A., 2005, A mid Mesozoic revolution in the regulation of ocean
1531 chemistry: Marine Geology, v. 217, no. 3-4, p. 339-357.
- 1532 Ridgewell, A., Hargreaves, J. C., Edwards, N. R., Annan, J. D., Lenton, T. M., Marsh,
1533 R., Yool, A., and Watson, A., 2007, Marine geo-chemical data assimilation in
1534 an efficient Earth System Model of global biogeochemical cycling:
1535 Biogeosciences, 4, 87-104, doi:10.5194/bg-4-87-2007, 2007.
- 1536 Rose, E. F., Chaussidon, M., and France-Lanord, C., 2000, Fractionation of boron
1537 isotopes during erosion processes: the example of Himalayan rivers:
1538 Geochimica et Cosmochimica Acta, v. 64, no. 3, p. 397-408.

- 1539 Rose-Koga, E. F., Sheppard, S. M. F., Chaussidon, M., and Carignan, J., 2006, Boron
 1540 isotopic composition of atmospheric precipitations and liquid-vapour
 1541 fractionations: *Geochimica et Cosmochimica Acta*, v. 70, no. 7, p. 1603-1615.
- 1542 | [Sanyal, A., Hemming, N.G., Hanson, G.N., Broecker, W.S., 1995, Evidence for a](#)
 1543 [higher pH in the glacial ocean from boron isotopes in foraminifera: Nature,](#)
 1544 [373, p. 243-236](#)
- 1545 Sanyal, A., Bijma, J., Spero, H., and Lea, D. W., 2001, Empirical relationship
 1546 between pH and the boron isotopic composition of *Globigerinoides sacculifer*:
 1547 Implications for the boron isotope paleo-pH proxy: *Paleoceanography*, v. 16,
 1548 no. 5, p. 515-519.
- 1549 | Schlitzer, R., Ocean Data View, [2016](#), <http://www.awi-bremerhaven.de/GEO/ODV>.
- 1550 Seki, O., Foster, G. L., Schmidt, D. N., Mackensen, A., Kawamura, K., and Pancost,
 1551 R. D., 2010, Alkenone and boron-based Pliocene $p\text{CO}_2$ records: *Earth and*
 1552 *Planetary Science Letters*, v. 292, no. 1-2, p. 201-211.
- 1553 Shipboard Scientific Party, 1989, Site 758. In Pearce, J., Weissel, J., et al., *Proc.
 1554 ODP, Init. Repts.*, 121: College Station, TX (Ocean Drilling Program), 359-
 1555 453. doi:10.2973/odp.proc.ir.121.112.1989
- 1556 Shipboard Scientific Party, 1995, Site 926. In Curry, W.B., Shackleton, N.J., Richter,
 1557 C., et al., *Proc. ODP, Init. Repts.*, 154: College Station, TX (Ocean Drilling
 1558 Program), 153-232. doi:10.2973/odp.proc.ir.154.105.1995
- 1559 Shipboard Scientific Party, 1997, Site 999. In Sigurdsson, H., Leckie, R.M., Acton,
 1560 G.D., et al., *Proc. ODP, Init. Repts.*, 165: College Station, TX (Ocean Drilling
 1561 Program), 131-230. doi:10.2973/odp.proc.ir.165.104.1997.
- 1562 Sigman, D.M., McCorkle, D.C., Martin, W.R., 1998, The calcite lysocline as a
 1563 constraint on glacial/interglacial low-latitude production changes: *Global
 1564 Biogeochem. Cycles*, v. 12, no. 3, p. 409-427.
- 1565 Simon, L., Lecuyer, C., Marechal, C., and Coltice, N., 2006, Modelling the
 1566 geochemical cycle of boron: Implications for the long-term $\delta^{11}\text{B}$ evolution of
 1567 seawater and oceanic crust: *Chemical Geology*, v. 225, no. 1-2, p. 61-76.
- 1568 Smith, H. J., Spivack, A. J., Staudigel, H., and Hart, S. R., 1995, The boron isotopic
 1569 composition of altered oceanic crust: *Chemical Geology*, v. 126, no. 2, p. 119-
 1570 135.
- 1571 Sosdian, S.M., Greenop, R., Lear, C.H., Foster, G.L., Hain, M.P., and Pearson, P.N.,
 1572 2015, Future ocean acidification could be unprecedented in the last 14 million
 1573 years: [in prep.](#)
- 1574 Spero, H., Mielke, K., Kalve, E., Lea, D., and Pak, D., 2003, Multispecies approach
 1575 to reconstructing eastern equatorial Pacific thermocline hydrography during
 1576 the past 360 kyr: *Paleoceanography*, v. 18, no. 1,
 1577 doi:10.1029/2001GC000200.
- 1578 Spezzaferri S, Kucera M, Pearson PN, Wade BS, Rappo S, Poole CR, et al., 2015,
 1579 Fossil and genetic evidence for the polyphyletic nature of the planktonic
 1580 foraminifera "*Globigerinoides*", and description of the new Genus *Trilobatus*:
 1581 PLoS ONE, v.10, no. 5, DOI:e0128108. doi:10.1371/journal.pone.0128108
- 1582 Spivack, A. J., and Edmond, J. M., 1987, Boron isotope exchange between seawater
 1583 and the oceanic crust: *Geochimica et Cosmochimica Acta*, v. 51, no. 5, p.
 1584 1033-1043.
- 1585 | [Takahashi, T., Sutherland S.C., Wanninkhof, R., Sweeney, C., Feely, R.A., et al.,](#)
 1586 [2009, Climatological mean and decadal change in surface ocean \$p\text{CO}_2\$, and](#)
 1587 [net sea-air \$\text{CO}_2\$ flux over global oceans: Deep-Sea Research II](#), v.56, p.554-
 1588 557.

r.greenop 12/8/2016 15:03

Deleted: 2010

r.greenop 6/9/2016 13:46

Deleted: submitted to Nature

- 1591 Tipper, E. T., Galy, A., and Bickle, M. J., 2006a, Riverine evidence for a fractionated
 1592 reservoir of Ca and Mg on the continents: Implications for the oceanic Ca
 1593 cycle: *Earth and Planetary Science Letters*, v. 247, no. 3–4, p. 267-279.
 1594 Tipper, E. T., Galy, A., Gaillardet, J., Bickle, M. J., Elderfield, H., and Carder, E. A.,
 1595 2006b, The magnesium isotope budget of the modern ocean: Constraints from
 1596 riverine magnesium isotope ratios: *Earth and Planetary Science Letters*, v.
 1597 250, no. 1–2, p. 241-253.
 1598 Tomascak, P. B., 2004, Developments in the Understanding and Application of
 1599 Lithium Isotopes in the Earth and Planetary Sciences: *Reviews in Mineralogy*
 1600 and *Geochemistry*, v. 55, no. 1, p. 153-195.
 1601 Tyrrell, T., and Zeebe, R. E., 2004, History of carbonate ion concentration over the
 1602 last 100 million years: *Geochimica Et Cosmochimica Acta*, v. 68, no. 17, p.
 1603 3521-3530.
 1604 Vengosh, A., Starinsky, A., Kolodny, Y., Chivas, A. R., and Raab, M., 1992, Boron
 1605 Isotope Variations during Fractional Evaporation of Sea-Water - New
 1606 Constraints on the Marine Vs Nonmarine Debate: *Geology*, v. 20, no. 9, p.
 1607 799-802.
 1608 Wimpenny, J., Colla, C. A., Yin, Q.-Z., Rustad, J. R., and Casey, W. H., 2014,
 1609 Investigating the behaviour of Mg isotopes during the formation of clay
 1610 minerals: *Geochimica et Cosmochimica Acta*, v. 128, no. 0, p. 178-194.
 1611 Wombacher, F., Eisenhauer, A., Böhm, F., Gussone, N., Regenberg, M., Dullo, W.
 1612 C., and Rüggeberg, A., 2011, Magnesium stable isotope fractionation in
 1613 marine biogenic calcite and aragonite: *Geochimica et Cosmochimica Acta*, v.
 1614 75, no. 19, p. 5797-5818.
 1615 You, C.F., Spivack, A. J., Smith, J. H., and Gieskes, J. M., 1993, Mobilization of
 1616 boron in convergent margins: Implications for the boron geochemical cycle:
 1617 *Geology*, v. 21, no. 3, p. 207-210.
 1618 Zeebe, R. E., and Wolf-Gladrow, D. A., 2001, CO₂ in seawater, equilibrium, kinetics,
 1619 isotopes IN Elsevier oceanography series, Amsterdam, PAYS-BAS, Elsevier,
 1620 XIII, 346 p. p.:
 1621 Zeeden, C., Hilgen, F., Westerhold, T., Lourens, L., Röhl, U., and Bickert, T., 2013,
 1622 Revised Miocene splice, astronomical tuning and calcareous plankton
 1623 biochronology of ODP Site 926 between 5 and 14.4 Ma: *Palaeogeography,*
 1624 *Palaeoclimatology, Palaeoecology*, v. 369, no. 0, p. 430-451.
 1625

1626

1627 **Figure Captions:**

- 1628 | Figure 1: The oceanic boron cycle. Fluxes are from Lemarchand et al. (2000) and
 1629 Park and Schlesinger (2002). Isotopic compositions are from Lemarchand et al.
 1630 | (2000), Foster et al., (2010) and references therein.
 1631 Figure 2: A compilation of published $\delta^{11}\text{B}_{\text{sw}}$ records. Seawater composition
 1632 reconstructed from foraminifera depth profiles (light blue squares and dark blue
 1633 cross) from Pearson and Palmer (2000) and Foster et al. (2012) respectively,

r.greenop 26/7/2016 19:37
Deleted: 2

r.greenop 26/7/2016 19:37
Deleted: 2

1636 numerical modelling (green line), with additional green lines shows $\pm 1\text{‰}$
1637 confidence interval (Lemarchand et al., 2000), benthic $\delta^{11}\text{B}$ (purple diamonds and
1638 dark purple line is using the fractionation factor of Klochko et al., 2006, light purple
1639 line using an empirical calibration) from Raitzsch and Hönisch (2013), and halites
1640 (orange crosses) from Paris et al. (2010). The orange crosses in brackets were
1641 discarded from the original study.▼

r.greenop 6/9/2016 12:12

Deleted: dark

r.greenop 26/7/2016 19:37

Deleted: 2

1642 Figure 3: Schematic diagram showing the change in pH gradient with a 3‰ change in
1643 $\delta^{11}\text{B}$ for $\delta^{11}\text{B}_{\text{sw}}$ of a) 39.6‰ and b) 37.5‰. Arrows highlight the different pH
1644 gradients. Note how a $\delta^{11}\text{B}$ difference of 3‰ is translated into different pH gradients
1645 depending on the $\delta^{11}\text{B}_{\text{sw}}$. Calculated using $B_T = 432.6 \mu\text{mol/kg}$ (Lee et al., 2010) and
1646 $\alpha_B = 1.0272$ (Klochko et al., 2006). (c) The pH change for a $\delta^{11}\text{B}$ change of 3‰ at a
1647 range of different $\delta^{11}\text{B}_{\text{sw}}$.

r.greenop 21/7/2016 10:26

Deleted: All the published $\delta^{11}\text{B}_{\text{sw}}$ curves are adjusted so that at $t=0$, the isotopic composition is equal to the modern (39.61‰).

1648 Figure 4: Map of study sites and mean annual air-sea disequilibria with respect to
1649 $p\text{CO}_2$. The black dots indicate the location of the sites used in this study. ODP Sites
1650 758, 999, 926 and 761 used in this study are highlighted with water depth. Data are
1651 from (Takahashi et al., 2009) plotted using ODV (Schlitzer, 2016).

r.greenop 12/8/2016 15:02

Formatted: Line spacing: 1.5 lines

1652 Figure 5: Latitudinal cross-section through the Atlantic showing (a) pH variations;
1653 (b) the $\delta^{13}\text{C}$ composition. Data are plotted using Ocean Data View (Schlitzer 2016).
1654 pH data are from the CARINA dataset (CARINA group, 2009) and the $\delta^{13}\text{C}$ data are
1655 from the GLODAP data compilation (Key et al., 2004); (c) pH and $\delta^{13}\text{C}_{\text{DIC}}$
1656 relationships in the modern ocean adapted from Foster et al., (2012). Because of
1657 anthropogenic acidification and the Suess effect only data from >1500 m are plotted.
1658 Also included in the plot are the data from a transect in the North Atlantic (from 0 to
1659 5000 m) where the effects of anthropogenic perturbation on both parameters have
1660 been corrected (Olsen and Ninneman, 2010).

r.greenop 21/7/2016 10:13

Deleted: 4

r.greenop 6/9/2016 12:19

Deleted: 2001

r.greenop 15/7/2016 12:36

Deleted: e

1661 Figure 6: $\delta^{11}\text{B}_{\text{planktic}}$, temperature and $\delta^{13}\text{C}_{\text{DIC}}$ estimates for the surface and deep
1662 ocean through the last 23 million years. (a) $\delta^{11}\text{B}_{\text{planktic}}$ surface; (b) $\delta^{11}\text{B}_{\text{borate}}$ deep from
1663 benthic foraminifera (blue) from this study and (green) Raitzsch and Hönisch, (2013).
1664 The error bars show the analytical external reproducibility at 95% confidence; (c)
1665 Mg/Ca based temperature reconstructions of surface dwelling planktic foraminifera;
1666 (d) Deep water temperature estimates from Cramer et al. (2011); (e) $\delta^{13}\text{C}_{\text{DIC}}$ surface
1667 record; (f) $\delta^{13}\text{C}_{\text{DIC}}$ benthic record. Squares depict ODP Site 999, triangles are ODP

r.greenop 21/7/2016 10:13

Deleted: 5

r.greenop 21/7/2016 10:17

Deleted: $\delta^{11}\text{B}_{\text{borate}}$

r.greenop 21/7/2016 10:17

Deleted: $\delta^{11}\text{B}_{\text{borate}}$

r.greenop 6/9/2016 12:34

Deleted: deep

r.greenop 15/7/2016 12:38

Deleted: calculated on paired measurements

1681 Site 758, diamonds are ODP Site 926, circles are ODP Site 761. Species are
 1682 highlighted by colour: Orange are *T. trilobus*, purple *G. ruber*, red *G. praebulloides*,
 1683 dark blue *Cibicidoides wuellestorfi* and light blue *Cibicidoides mundulus*. The two
 1684 benthic-planktic pairs that were removed prior to smoothing are highlighted with
 1685 arrows.
 1686 Figure 7; The output from GENIE sensitivity analysis showing the warm-surface-to-
 1687 cold-deep ΔpH -to- $\Delta\delta^{13}\text{C}$ relationship. A pre-industrial model setup was taken and
 1688 perturbations were made to alkalinity inventory, carbon inventory, Antarctic shelf
 1689 fresh water flux (Sv), Atlantic-Pacific freshwater flux, S. Lim gas exchange (blocks
 1690 air-sea gas exchange south of the stated latitude), remineralisation depth scale (m)
 1691 and rain ratio – as described in the methods section. Blue circles depict the ΔpH -to-
 1692 $\Delta\delta^{13}\text{C}$ relationship (where the colours reflect the CO₂ level of each experiment) and
 1693 red open circles show the root mean square of the regression (RMSE). The green
 1694 stars are the ΔpH -to- $\Delta\delta^{13}\text{C}$ relationship for the control experiment conducted at
 1695 292.67 ppm CO₂. The green (open) points show the RMSE for this control run.
 1696 Inventories are dimensionless (1 is control). For the Atlantic-Pacific FWF 1 is
 1697 equivalent to 0.32 Sv. The alkalinity and carbon inventory experiments are very
 1698 extreme and inconsistent with geologic evidence.
 1699 Figure 8; The output from sensitivity analysis of the relationship between pH gradient
 1700 and $\delta^{13}\text{C}$ gradient from the 13500 run CYCLOPS ensemble (see text for model
 1701 details). Panel (a) shows the mean gradient when the result from all 18 ocean boxes
 1702 are included in the regression. Panel (b) shows only the boxes from the low latitude
 1703 ocean from all basins and (c) shows the regression from only North Atlantic low
 1704 latitude boxes. Note the lower $\Delta\text{pH}/\Delta\delta^{11}\text{B}$ slope at the lower latitudes due to the
 1705 effect of temperature.
 1706 Figure 9; The pH gradient between surface and deep through time calculated from the
 1707 $\delta^{13}\text{C}$ gradient and using a flat probability derived from the low latitude ensemble
 1708 regressions from the CYCLOPS model. The modern pH gradients at each site are
 1709 also plotted.
 1710 Figure 10; The calculated $\delta^{11}\text{B}_{\text{sw}}$ from the benthic-planktic $\delta^{11}\text{B}$ pairs using a pH
 1711 gradient derived from $\delta^{13}\text{C}$. The uncertainty on each data point is determined using a
 1712 Monte Carlo approach including uncertainties in temperature, salinity, $\delta^{11}\text{B}$ and the

r.greenop 21/7/2016 10:13
Deleted: 6
r.greenop 17/8/2016 18:13
Deleted: of the relationship between pH gradient and $\delta^{13}\text{C}$ gradient from GENIE
r.greenop 17/8/2016 18:13
Deleted: The gradient of a linear regression for each experiment, with $\delta^{13}\text{C}$ and pH data taken from each grid square, is plotted.
r.greenop 17/8/2016 18:13
Deleted: gradient
r.greenop 5/9/2016 19:02
Deleted: data points (closed)
r.greenop 17/8/2016 18:15
Deleted:
r.greenop 17/8/2016 18:14
Deleted: gradient of the linear regression
r.greenop 17/8/2016 18:14
Deleted: All other sensitivity test indicate a possible range from 0.195 to 0.205 for the slope of the pH/ $\delta^{13}\text{C}$ regression.
r.greenop 21/7/2016 10:13
Deleted: 7
r.greenop 17/8/2016 18:09
Deleted: 13700
r.greenop 21/7/2016 10:13
Deleted: 8
r.greenop 21/7/2016 10:26
Deleted: the
r.greenop 21/7/2016 10:26
Deleted: whole ocean (blue) (panel (a) Fig. 7),
r.greenop 21/7/2016 10:27
Deleted: (green) (panel (b) Fig. 7) and low latitude North Atlantic only (red) (panel (c) Fig. 7) based
r.greenop 21/7/2016 10:13
Deleted: 9
r.greenop 26/7/2016 19:40
Deleted: assuming
r.greenop 26/7/2016 19:39
Deleted: (a)
r.greenop 26/7/2016 19:39
Deleted: (a) the modern pH (blue); (b)
r.greenop 26/7/2016 19:40
Deleted: (red)

1740 pH gradient (see text for details). Data are plotted as box and whisker diagrams
1741 where the median and interquartile range as plotted in the box and whiskers show the
1742 maximum and minimum output from the Monte Carlo simulations. The line of best
1743 fit is the probability maximum of a LOWESS fit given the uncertainty in the
1744 calculated $\delta^{11}\text{B}_{\text{sw}}$. The darker shaded area highlights the 68% confidence interval and
1745 the lighter interval highlights the 95% confidence interval. The bottom panel shows
1746 box plots of the mean and 2 standard error (s.e.) of ‘binning’ the individual $\delta^{11}\text{B}_{\text{sw}}$
1747 measurements into 8 Myr intervals. The middle line is the mean and the box shows
1748 the 2 s.e. of the data points in that bin. The smoothed record is also plotted for
1749 comparison where the line of best fit is the probability maximum of a LOWESS fit
1750 given the uncertainty in the calculated $\delta^{11}\text{B}_{\text{sw}}$. The darker shaded area highlights the
1751 68% confidence interval and the lighter interval highlights the 95% confidence
1752 interval. The black dot is the modern value of 39.61 ‰ (Foster et al., 2010).

1753 Figure 1¹; The $\delta^{11}\text{B}_{\text{sw}}$ curve calculated using the variable pH gradient derived from
1754 $\delta^{13}\text{C}$. The median (red line), 68% (dark red band) and 95% (light red band)
1755 confidence intervals are plotted. Plotted with a compilation of published $\delta^{11}\text{B}_{\text{sw}}$
1756 records. Seawater composition reconstructed from foraminifera depth profiles (light
1757 blue squares and dark blue cross) from Pearson and Palmer (2000) and Foster et al.
1758 (2012) respectively, numerical modelling (green line), with additional green green
1759 lines shows ± 1 ‰ confidence interval (Lemarchand et al., 2000) and benthic $\delta^{11}\text{B}$
1760 (purple diamonds and dark purple line is using the fractionation factor of Klochko et
1761 al., 2006, light purple line using an empirical calibration) from Raitzsch and Hönnisch
1762 (2013). All the published $\delta^{11}\text{B}_{\text{sw}}$ curves are adjusted so that at t=0, the isotopic
1763 composition is equal to the modern (39.61 ‰).

1764 Figure 1²; a) The $\delta^{11}\text{B}_{\text{sw}}$ curve from this study plotted with other trace element
1765 isotopic records. On the $\delta^{11}\text{B}_{\text{sw}}$ panel, the darker shaded area highlights the 68%
1766 confidence interval and the lighter interval highlights the 95% confidence interval),
1767 $\delta^{26}\text{Mg}_{\text{sw}}$ record from Pogge von Strandmann et al. (2014) (error bars are ± 0.28 ‰
1768 and include analytical uncertainty and scatter due to the spread in modern *O. universa*
1769 and the offset between the two analysed species), $\delta^{44/40}\text{Ca}_{\text{sw}}$ record from Griffith et al.
1770 (2008) (error bars show 2 σ uncertainty) and $\delta^7\text{Li}_{\text{sw}}$ record from Misra and Froelich
1771 (2012) (error bars show 2 σ uncertainty). Blue dashed lines show middle Miocene
1772 values, red dashed lines highlight the modern.

r.greenop 26/7/2016 19:42
Deleted: The circles highlight the data points that were removed prior to LOWESS smoothing; (c)

r.greenop 12/8/2016 12:31
Deleted: an expanded view of the smoothed

r.greenop 26/7/2016 19:41
Deleted: curves for ease of comparison between the variable pH gradient from $\delta^{13}\text{C}$ (red) and modern pH gradient (blue).
r.greenop 21/7/2016 10:13
Deleted: 0
r.greenop 26/7/2016 19:39
Deleted: a)

r.greenop 6/9/2016 12:38
Deleted: dark
r.greenop 26/7/2016 19:37
Deleted: 2
r.greenop 21/7/2016 10:28
Deleted: line

r.greenop 21/7/2016 10:13
Deleted: 1
r.greenop 6/9/2016 12:39
Deleted: calculated using the variable pH gradient derived from $\delta^{13}\text{C}$
r.greenop 6/9/2016 12:39
Deleted: (

1789 | Figure 13: Crossplots of the records of $\delta^{11}\text{B}_{\text{sw}}$ using the variable pH gradient derived
1790 | from $\delta^{13}\text{C}$ (error bars show 2σ uncertainty) with $\delta^{44/40}\text{Ca}_{\text{sw}}$ from Griffith et al. (2008)
1791 | (error bars show 2σ uncertainty), $\delta^7\text{Li}_{\text{sw}}$ from Misra and Froelich (2012) (error bars
1792 | show 2σ uncertainty) and $\delta^{26}\text{Mg}_{\text{sw}}$ from Pogge von Strandmann et al. (2014) (error
1793 | bars are $\pm 0.28\text{‰}$ and include analytical uncertainty and scatter due to the spread in
1794 | modern *O. universa* and the offset between the two analysed species). The colour of
1795 | the data points highlights the age of the data points where red = modern and blue =
1796 | 23 Ma.

r.greenop 21/7/2016 10:13
Deleted: 2

1797 | [Table 1: CYCLOPS model parameter values defining the ensemble of 13,500](#)
1798 | [simulations.](#)

1799 | [Table 2: Uncertainty inputs into the Monte Carlo simulations to calculate \$\delta^{11}\text{B}\$. The](#)
1800 | [sources of uncertainty are also added. All uncertainty estimates are \$2\sigma\$.](#)

1801 | Table 3: The average $\delta^{11}\text{B}$, $\delta^{26}\text{Mg}$, $\delta^{44/40}\text{Ca}$ and $\delta^7\text{Li}$ composition of major fluxes into
1802 | and out of the ocean. Colour coding reflects the relative importance of each the
1803 | processes (darker shading reflects greater importance). The colour coding for boron is
1804 | based on Lemarchand et al. (2000) and references therein, lithium from Misra and
1805 | Froelich (2012) and references therein, magnesium from Tipper et al. (2006b) and
1806 | calcium from Fantle and Tipper (2014) and Griffin et al. (2008) and references
1807 | therein. The isotopic ratio of each process is: (a) Lemarchand et al. (2000) and
1808 | references therein; b) Misra and Froelich (2012) and references therein; (c) Burton
1809 | and Vigier (2012); (d) Tipper et al. (2006b); e) Wombacher et al. (2011); f) includes
1810 | dolomitisation; g) removal through hydrothermal activity; h) Griffith et al. (2008); i)
1811 | Fantle and Tipper (2014) and references therein; j) dolomitisation may be an
1812 | important component of the carbonate flux. Modern $\delta^{26}\text{Mg}_{\text{sw}}$ and $\delta^{11}\text{B}_{\text{sw}}$ from Foster
1813 | et al. (2010), $\delta^7\text{Li}_{\text{sw}}$ from Tomascak (2004). The $\delta^{44/40}\text{Ca}$ presented here was
1814 | measured relative to seawater and hence seawater has a $\delta^{44/40}\text{Ca}_{\text{sw}}$ of 0 permil by
1815 | definition.

r.greenop 21/7/2016 10:13
Deleted: 1

1816

r.greenop 26/7/2016 19:37
Deleted: 2

r.greenop 26/7/2016 19:37
Deleted: 2

Page 3: [1] Deleted r.greenop 26/07/2016 19:37

2

Page 3: [2] Formatted r.greenop 11/08/2016 14:29

Superscript

Page 3: [3] Deleted r.greenop 11/08/2016 14:27

such that seawater is isotopically heavier (39.61‰) than the inputs (which average at 10.4‰).

Page 3: [3] Deleted r.greenop 11/08/2016 14:27

such that seawater is isotopically heavier (39.61‰) than the inputs (which average at 10.4‰).

Page 3: [3] Deleted r.greenop 11/08/2016 14:27

such that seawater is isotopically heavier (39.61‰) than the inputs (which average at 10.4‰).

Page 3: [4] Formatted	r.greenop	11/08/2016 14:38
------------------------------	-----------	------------------

Font:(Default) Times, 12 pt, Not Bold

Page 3: [4] Formatted	r.greenop	11/08/2016 14:38
------------------------------	-----------	------------------

Font:(Default) Times, 12 pt, Not Bold

Page 3: [4] Formatted	r.greenop	11/08/2016 14:38
------------------------------	-----------	------------------

Font:(Default) Times, 12 pt, Not Bold

Page 3: [5] Deleted	r.greenop	11/08/2016 14:35
----------------------------	-----------	------------------

Mg, Ca, Li, Sr

Page 3: [5] Deleted	r.greenop	11/08/2016 14:35
----------------------------	-----------	------------------

Mg, Ca, Li, Sr

Page 3: [5] Deleted	r.greenop	11/08/2016 14:35
----------------------------	-----------	------------------

Mg, Ca, Li, Sr

Page 3: [5] Deleted	r.greenop	11/08/2016 14:35
----------------------------	-----------	------------------

Mg, Ca, Li, Sr

Page 3: [5] Deleted	r.greenop	11/08/2016 14:35
----------------------------	-----------	------------------

Mg, Ca, Li, Sr

Page 3: [5] Deleted	r.greenop	11/08/2016 14:35
----------------------------	-----------	------------------

Mg, Ca, Li, Sr

Page 3: [5] Deleted	r.greenop	11/08/2016 14:35
----------------------------	-----------	------------------

Mg, Ca, Li, Sr

Page 3: [5] Deleted	r.greenop	11/08/2016 14:35
----------------------------	-----------	------------------

Mg, Ca, Li, Sr

Page 3: [5] Deleted r.greenop 11/08/2016 14:35
Mg, Ca, Li, Sr

Page 3: [5] Deleted r.greenop 11/08/2016 14:35
Mg, Ca, Li, Sr

Page 3: [5] Deleted r.greenop 11/08/2016 14:35
Mg, Ca, Li, Sr

Page 3: [5] Deleted r.greenop 11/08/2016 14:35
Mg, Ca, Li, Sr

Page 3: [5] Deleted r.greenop 11/08/2016 14:35
Mg, Ca, Li, Sr

Page 4: [6] Deleted r.greenop 08/06/2016 21:01
Yet brine-halite fractionation offsets of -20‰ to -30‰ and -5‰ are reported from laboratory and natural environments respectively casting doubt over the validity of the assumption that no fractionation occurs during halite formation (Vengosh et al., 1992; Liu et al., 2000). These fractionations and riverine input during basin isolation will drive the evaporite-hosted boron to low- $\delta^{11}\text{B}$ isotope values such that the fluid inclusion record likely provides a lower limit for the $\delta^{11}\text{B}_{\text{sw}}$ through time (i.e. $\delta^{11}\text{B}_{\text{sw}}$ is heavier than the halite fluid inclusions of Paris et al. (2010)). Nevertheless, evaporites form from modified seawater in isolated basins making them unlikely archives of representative ocean $\delta^{11}\text{B}$.

Page 4: [7] Deleted r.greenop 11/08/2016 14:53
An alternative semi-empirical approach makes assumptions regarding the evolution of Cenozoic deep-ocean pH and a benthic $\delta^{11}\text{B}$ record to determine changes in $\delta^{11}\text{B}_{\text{sw}}$

Page 4: [8] Deleted r.greenop 11/08/2016 14:56
which can be converted to $\delta^{11}\text{B}_{\text{sw}}$ based on

Page 4: [9] Deleted r.greenop 18/07/2016 15:00

While this approach yields a qualitative independent check on other approaches (e.g. halite inclusions, geochemical modeling), as a quantitative record of $\delta^{11}\text{B}_{\text{sw}}$ through time, it has a number of drawbacks. Firstly, some of the CO₂ data used in the modeling studies is derived using the boron isotope-pH proxy, leading to some circularity in the methodology. Secondly, given the structure in CO₂ proxy records, the assumption that surface ocean pH changed linearly through the Cenozoic is most likely an oversimplification (Beerling and Royer, 2011). Consequently, while this method may shed some light on the evolution of $\delta^{11}\text{B}_{\text{sw}}$ through time, it cannot be subsequently used to determine pH or atmospheric CO₂ from $\delta^{11}\text{B}$ of foraminiferal calcite because the $\delta^{11}\text{B}_{\text{sw}}$ record is itself based on assumptions of the secular evolution of pH and CO₂.

One of the big challenges of reconstructing a

Page 4: [10] Deleted r.greenop 11/08/2016 14:59

record empirically is determining $\delta^{11}\text{B}_{\text{sw}}$

Page 4: [11] Deleted r.greenop 11/08/2016 15:00

One way to avoid using absolute pH reconstructions is to exploit the non-linear relationship between $\delta^{11}\text{B}$ and pH alongside estimated pH gradients in the ocean to constrain $\delta^{11}\text{B}_{\text{sw}}$.

Page 4: [12] Moved to page 18 (Move #3) r.greenop 18/07/2016 12:14

Unfortunately, the applicability of this $\delta^{11}\text{B}_{\text{sw}}$ record (derived from $\delta^{11}\text{B}$ data measured using NTIMS) to $\delta^{11}\text{B}$ records generated using the MC-ICPMS is uncertain (Foster et al., 2013). In addition, this $\delta^{11}\text{B}_{\text{sw}}$ record is determined using a fractionation factor of 1.0194 (Kakihana et al., 1977), whereas recent experimental data have shown the value to be higher (1.0272 ± 0.0006 , Klochko et al., 2006). Thirdly, given our understanding of the $\delta^{11}\text{B}$ difference between species/size fractions (Foster, 2008; Henehan et al., 2013), the mixed species and size fractions used to make the $\delta^{11}\text{B}$ measurements in that study may have introduced some additional uncertainty in the reconstructed $\delta^{11}\text{B}_{\text{sw}}$. Consequently, while the estimates from Pearson and Palmer (2000) show that the rationale behind this

approach can yield useful $\delta^{11}\text{B}_{\text{sw}}$ estimates that may be qualitatively correct, the underlying measurements and some of the key assumptions have led to uncertainties in the record.

Page 16: [13] Deleted

r.greenop

15/07/2016 16:15

The slope of the pH- $\delta^{13}\text{C}$ relationship simulated by our CYCLOPS model ensemble across a range of perturbed states is 0.2047 ($1\sigma = 0.0196$) (Fig. 7a, 8), in perfect agreement with modern empirical data and our GENIE experiments. Varying the biogeochemical parameters (gas exchange, rain ratio and remineralizing depth scale) yields some change in the regressed slope of the pH/ $\delta^{13}\text{C}$ relationship due to decoupled responses of pH and $\delta^{13}\text{C}$, but this gradient remains well within the 0.2 +/- 0.05 range, and a RMSE of 0.05 in the spatial relationship remains robust (Fig. 6). We take this as evidence that the uncertainty in the pH/ $\delta^{13}\text{C}$ relationship assumed in our carbon chemistry calculation is well represented by a central value of 0.2 with a 0.025 standard deviation. Experiments at very high DIC or low alkalinity, either of which yield high atmospheric $p\text{CO}_2$ and low mean ocean pH, yield gradients slightly outside the 0.2 +/- 0.05 range, with an elevated RMSE. This is probably associated with the non-linearity of the pH scale, modifying the gradient for a very different pH. It is to be emphasised that such extreme decoupled changes in DIC and alkalinity are not plausible within the Cenozoic, and were only possible in these simulations because of the absence of interactive sediments.

The slope of the pH- $\delta^{13}\text{C}$ relationship simulated by our CYCLOPS model ensemble across a range of perturbed states is 0.2047 ($1\sigma = 0.0196$) (Fig. 7a, 8), in perfect agreement with modern empirical data and our GENIE experiments. We take this agreement as evidence that the slope of the pH- $\delta^{13}\text{C}$ relationship is a feature of ocean biogeochemistry that is relatively conserved even if ocean carbon chemistry and circulation change drastically. For the purpose of calculating $\delta^{11}\text{B}_{\text{sw}}$ from our benthic/planktic foraminifera measurements we need to estimate the pH difference between the low latitude surface and deep ocean at the sample sites, most of which are in the subtropical North Atlantic. If we restrict our analysis of the CYCLOPS ensemble to only the low latitude surface boxes and the corresponding deep ocean boxes (i.e.,

Atlantic, Indian, South Pacific and North Pacific) the slope of the applicable pH- $\delta^{13}\text{C}$ relationship is 0.1797 ($1\sigma = 0.0213$) (Fig. 7b, 8), which is significantly less than the regression based on all 18 model boxes. Further, if only the Atlantic low latitude surface and deep ocean boxes are used to calculate the slope of the applicable pH- $\delta^{13}\text{C}$ relationship declines to 0.1655 ($1\sigma = 0.0192$) (Fig. 7c, 8). Thus, excluding the polar ocean and the ocean's mid-depth permanent thermocline from the analysis consistently yields a shallower slope of the pH- $\delta^{13}\text{C}$ relationship, with some evidence for water mass dependence also in the modern observations (Fig. 4). Here we calculate $\delta^{11}\text{B}_{\text{sw}}$ for all three estimates of the pH- $\delta^{13}\text{C}$ slope (global regression 0.201; low latitude surface and deep regression 0.1797; Atlantic low latitude surface to deep box gradients 0.1655) assuming a generous uncertainty of 0.05 (2 σ) in all cases, and we provide all three $\delta^{11}\text{B}_{\text{sw}}$ scenarios as an online supplement. Overall, the slope between pH and $\delta^{13}\text{C}$ is dependent on the competition between spatial variations in remineralized soft tissue, increasing the slope between pH and $\delta^{13}\text{C}$, and seawater temperature, decreasing the slope between pH and $\delta^{13}\text{C}$. The largest concentrations of remineralized soft tissue occur in the thermocline, suggesting that a relatively steep pH- $\delta^{13}\text{C}$ slope is appropriate for estimating the pH gradient from the $\delta^{13}\text{C}$ difference. However, when comparing surface to deep waters, as is done in this study, the full range of the temperature effect is expressed and a relatively shallow pH- $\delta^{13}\text{C}$ slope is appropriate. This is particularly true given that our samples are from the low latitude surface and the cold deep ocean. Since most of our measurements are from the subtropical Atlantic it is perhaps most appropriate to use the slope regressed from the low latitude surface and deep boxes from this ocean basin (i.e., $\Delta\text{pH}/\Delta\delta^{13}\text{C} = 0.1655$; with $1\sigma = 0.025$) and we will focus on those calculations in the following discussion (Fig. 9).

Page 16: [14] Deleted

r.greenop

18/07/2016 11:18

The individual $\delta^{11}\text{B}_{\text{sw}}$ estimates calculated using the modern pH gradient method vary from 34.9 ‰ to 42.2 ‰ (± 0.84 -4.77 ‰) across the Neogene with a predominance of higher values closer to the modern and lowest values in the middle Miocene (Fig. 9). After smoothing is applied to satisfy seawater B mass balance, the long-term $\delta^{11}\text{B}_{\text{sw}}$ is determined as 37.5 ‰ at 23 Ma, decreases to a minimum of 37.17 ‰ at ~ 13 Ma (± 0.34 -

1.81 ‰), and subsequently increases gradually towards modern values through the late Miocene, Pliocene and Pleistocene (Fig. 9). The variability in the estimations of $\delta^{11}\text{B}_{\text{sw}}$ for each individual benthic/planktic foraminifera pair suggest that individual estimates of $\delta^{11}\text{B}_{\text{sw}}$ are sensitive to the different input parameters, particularly the assigned uncertainty in the pH gradient. However, by smoothing the record we effectively suppress error that is uncorrelated between individual benthic/planktic pairs of similar age and thereby focus on the effect of changes in $\delta^{11}\text{B}_{\text{sw}}$ that are correlated over multi-million year timescales.

Page 16: [15] Moved to page 17 (Move #2)r.greenop

18/07/2016 11:18

The variability in the estimations of $\delta^{11}\text{B}_{\text{sw}}$ for each individual benthic/planktic foraminifera pair suggest that individual estimates of $\delta^{11}\text{B}_{\text{sw}}$ are sensitive to the different input parameters, particularly the assigned uncertainty in the pH gradient. However, by smoothing the record we effectively suppress error that is uncorrelated between individual benthic/planktic pairs of similar age and thereby focus on the effect of changes in $\delta^{11}\text{B}_{\text{sw}}$ that are correlated over multi-million year timescales.

Page 17: [16] Deleted

r.greenop

18/07/2016 11:24

When using $\delta^{13}\text{C}$ gradients as predictors for the pH gradient the $\delta^{11}\text{B}_{\text{sw}}$ values calculated are broadly similar to the results with assumed constant pH gradient: $\delta^{11}\text{B}_{\text{sw}}$ varies from 34.1 ‰ to 42.3 ‰ (± 0.72 -4.0 ‰) across the Neogene with the predominance of higher values closer to the modern with the lowest values in the middle Miocene (Fig. 9). However, when the individual $\delta^{11}\text{B}_{\text{sw}}$ estimates are smoothed, while the $\delta^{11}\text{B}_{\text{sw}}$ calculated using this method is similar to the constant pH gradient scenario through the late and middle Miocene ($\sim 37.5 \pm 0.19$ -1.28 ‰), the subsequent increase occurs more rapidly and the $\delta^{11}\text{B}_{\text{sw}}$ record reaches modern values by ~5 Ma (Fig. 9). The variability in the estimations of $\delta^{11}\text{B}_{\text{sw}}$ for each individual benthic/planktic foraminifera pair suggest that individual estimates of $\delta^{11}\text{B}_{\text{sw}}$ are sensitive to the different input parameters, particularly the assigned uncertainty in the pH gradient. However, by smoothing the record we effectively suppress error that is uncorrelated between individual benthic/planktic pairs of similar age and thereby focus on the effect of changes in $\delta^{11}\text{B}_{\text{sw}}$ that are correlated over multi-million year timescales.

Given the variability we observe in the $\delta^{13}\text{C}$ derived pH gradient, and the consistency between the modelled pH gradient using GENIE and CYCLOPS, we conclude using the benthic-to-planktic pH difference calculated using the $\delta^{13}\text{C}$ gradient is indeed an improvement over the assumption that pH gradients remained constant through time. Therefore, we recommend the use of the $\delta^{13}\text{C}$ -corrected $\delta^{11}\text{B}_{\text{sw}}$ moving forward and in the following discussion we will limit our attention to this record.

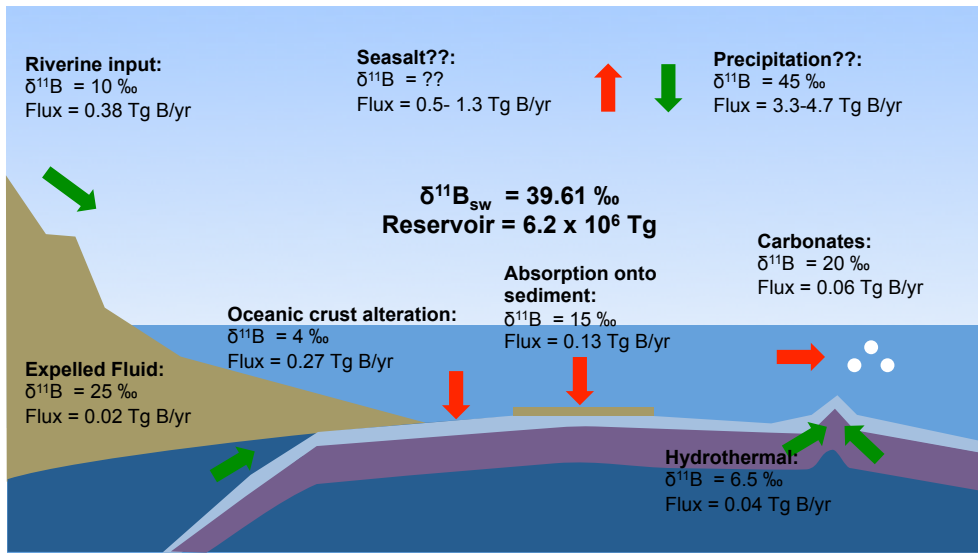


Figure 1

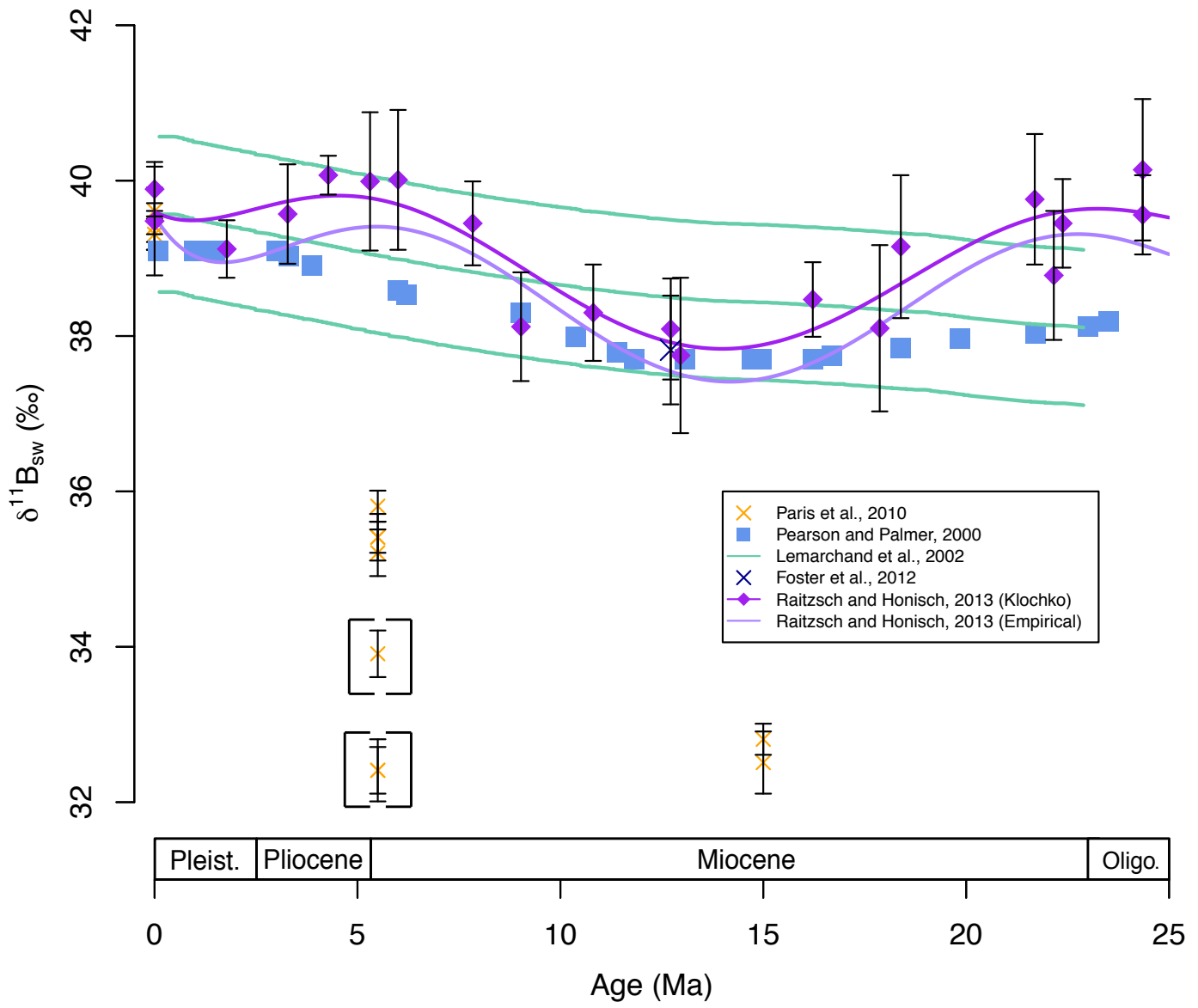


Figure 2

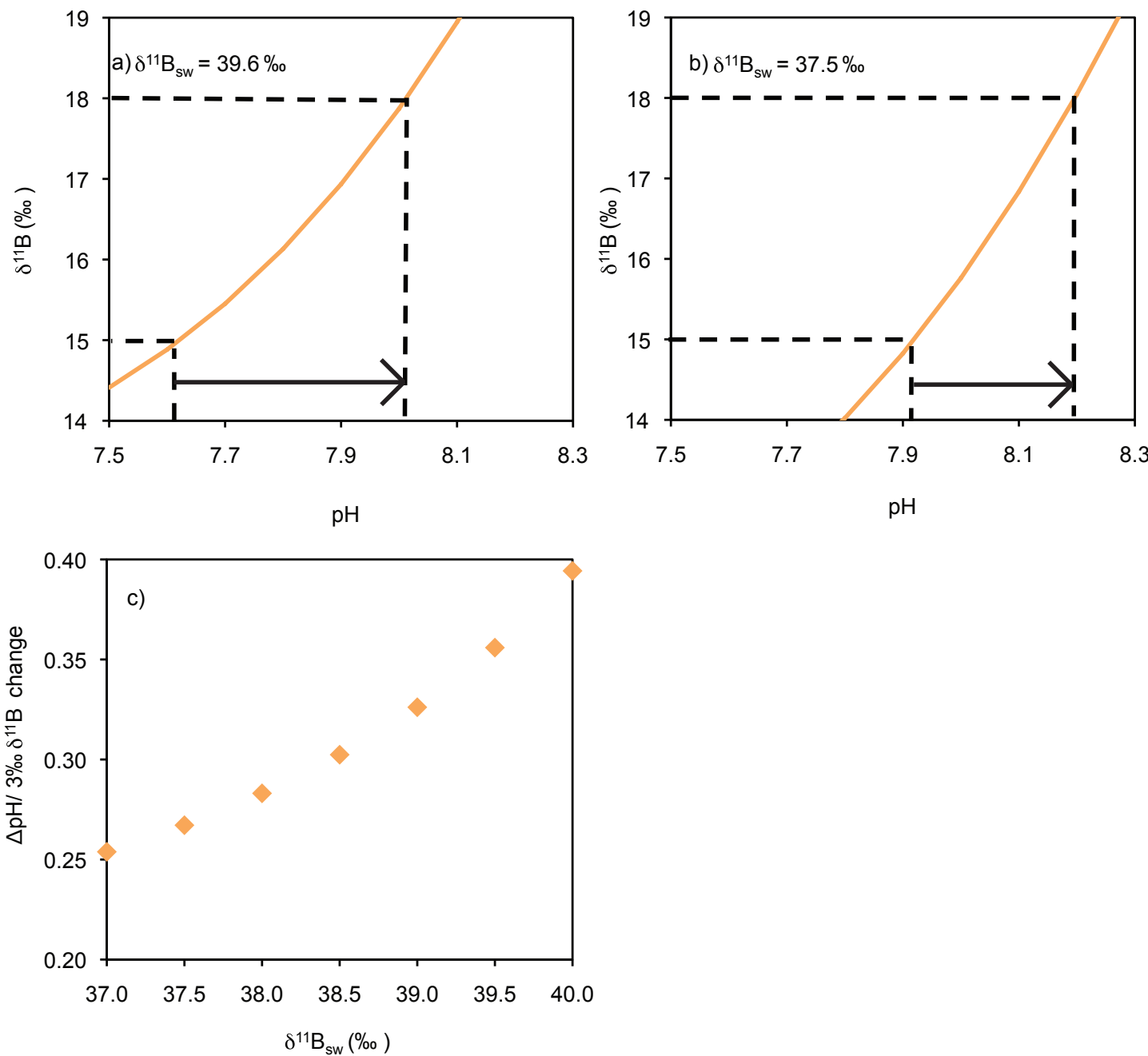


Figure 3

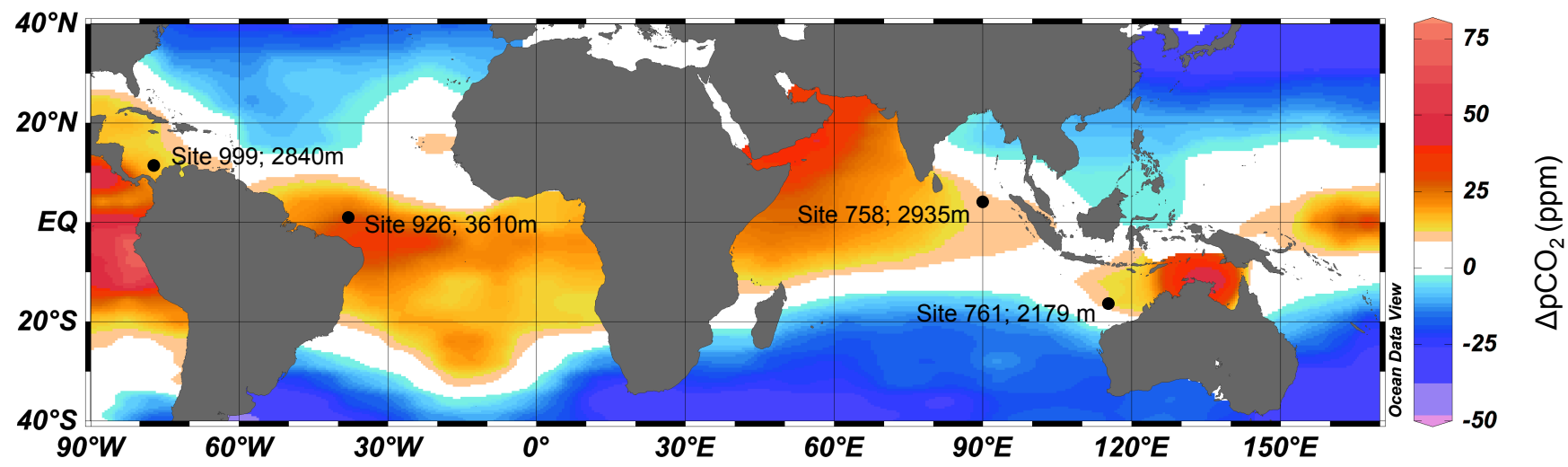


Figure 4

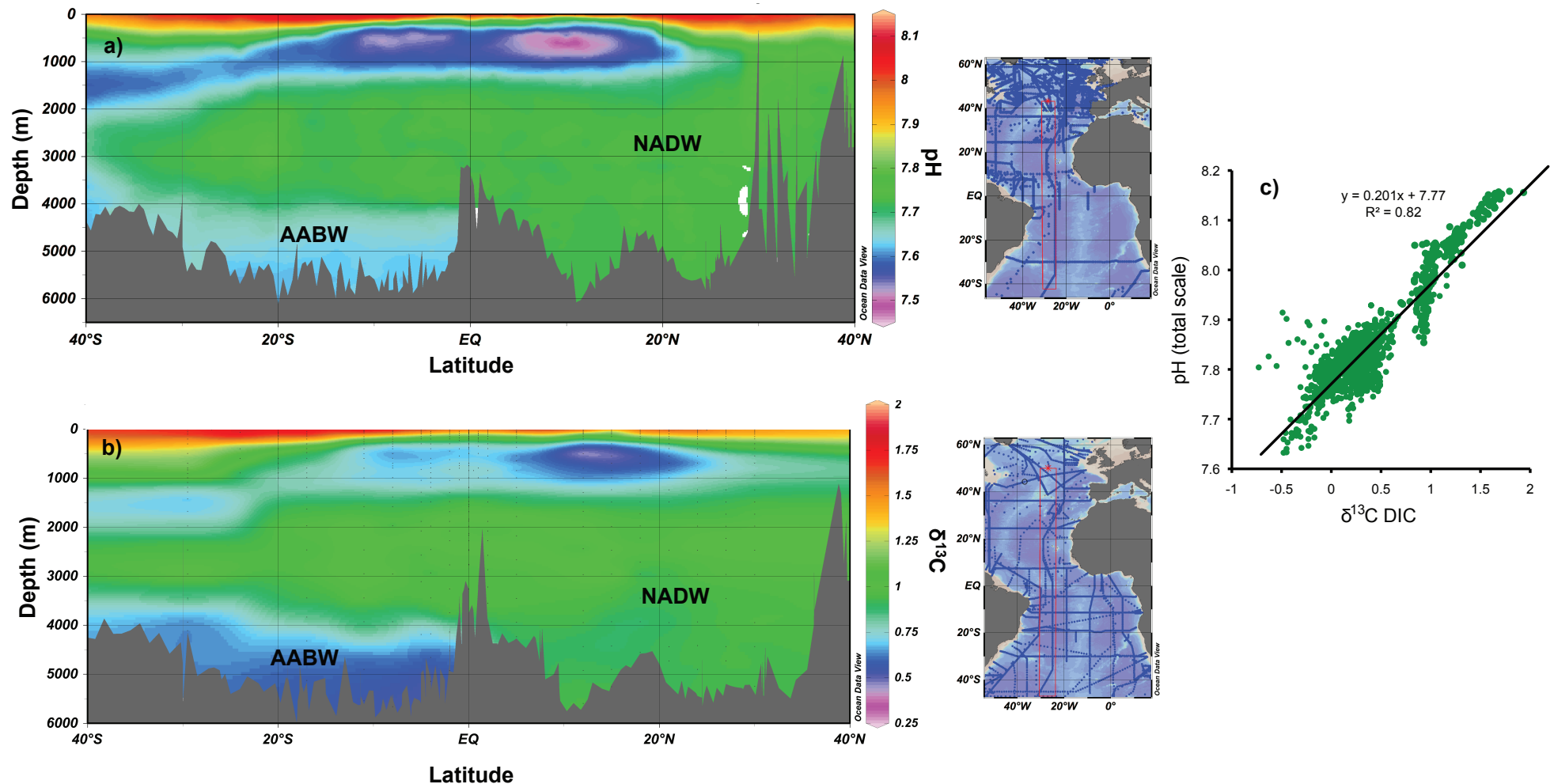
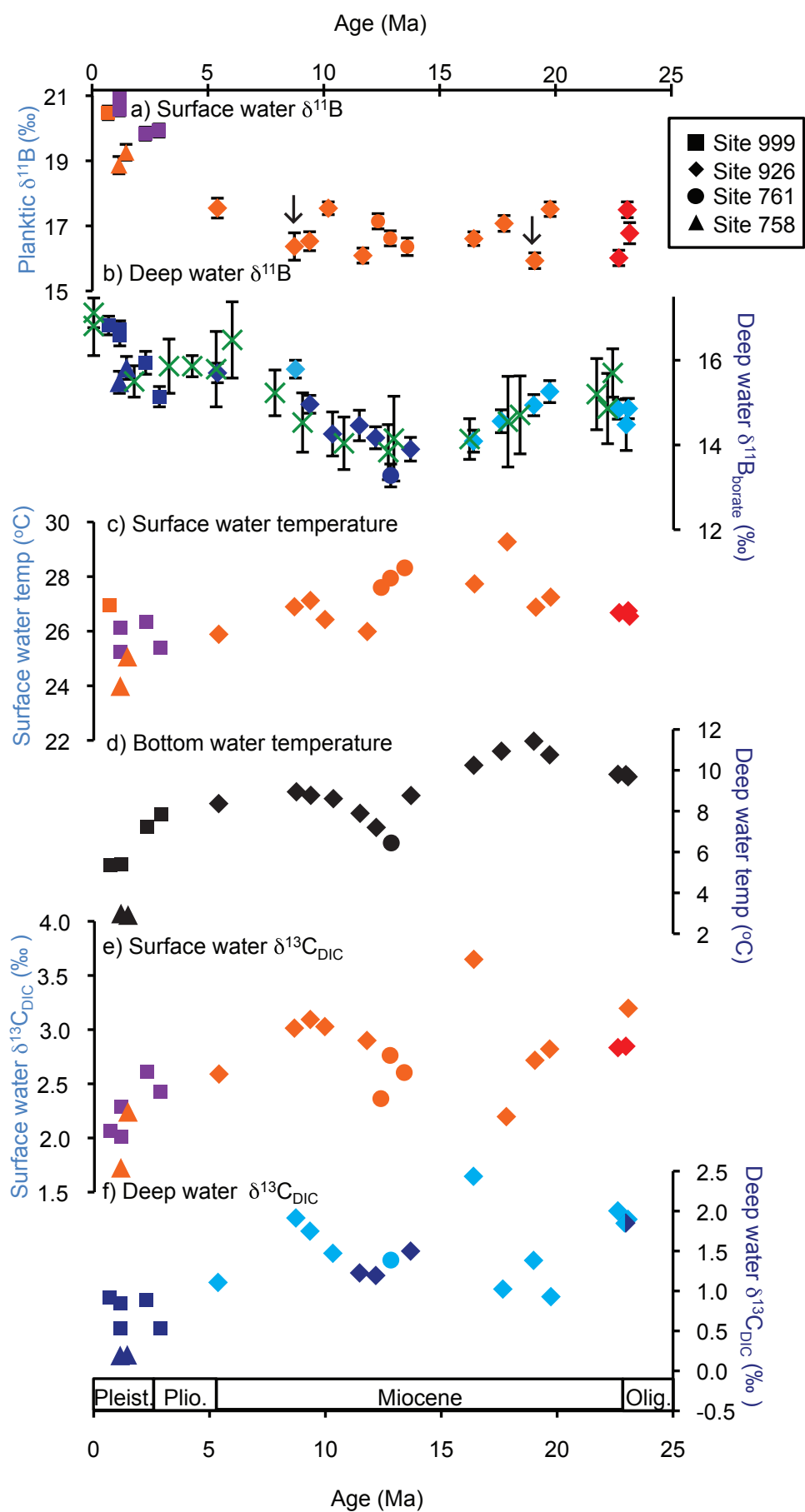


Figure 5

Figure 6



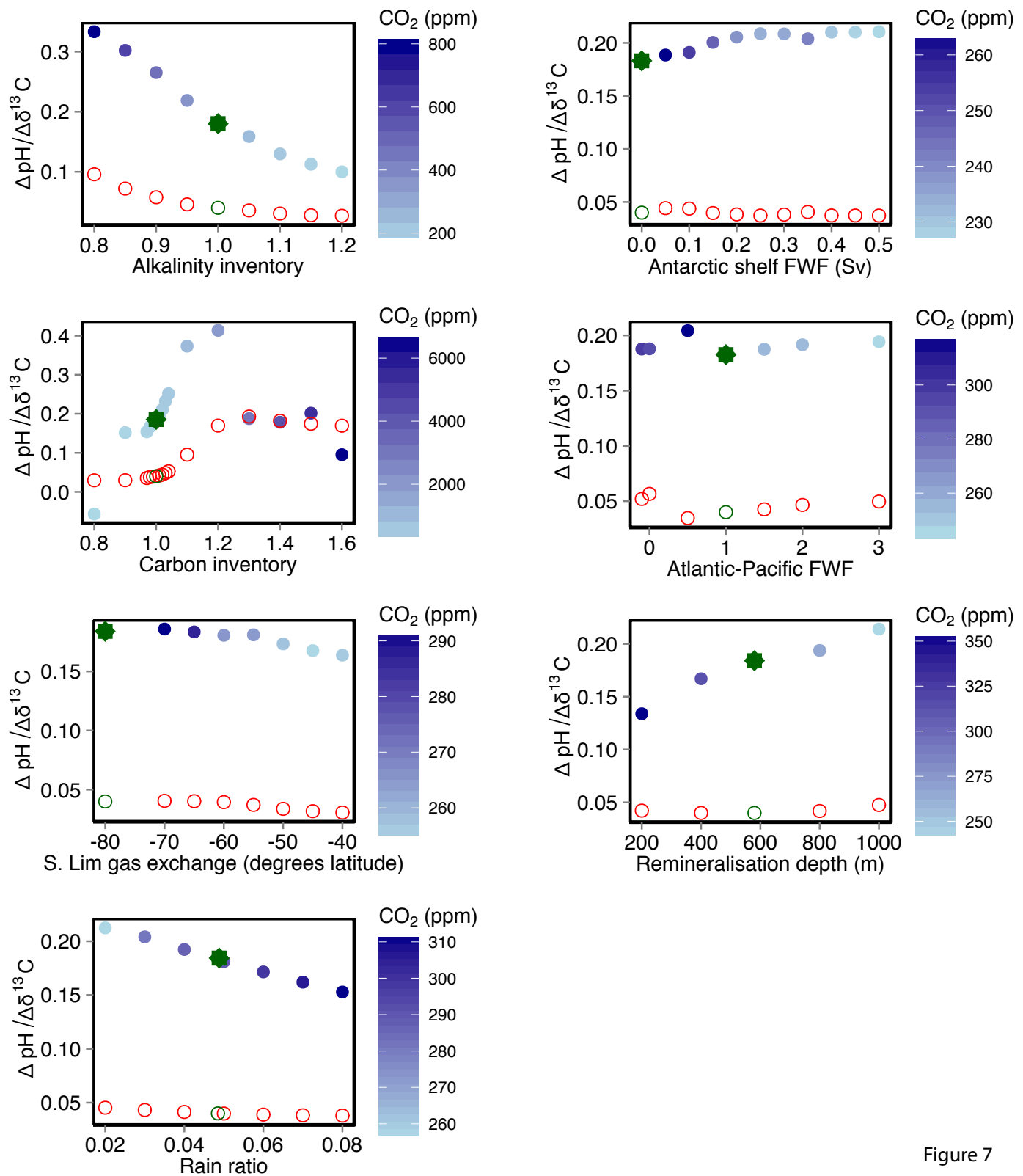


Figure 7

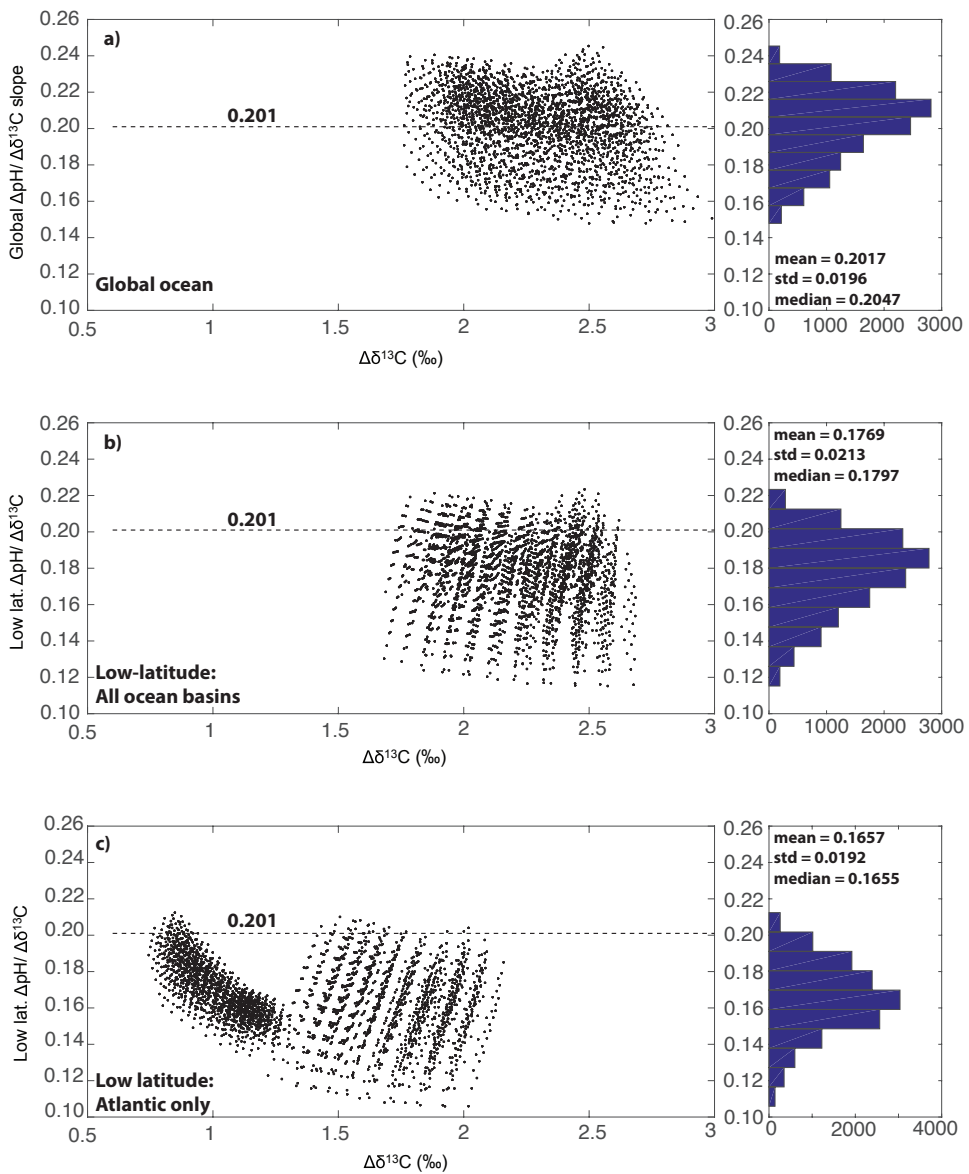


Figure 8

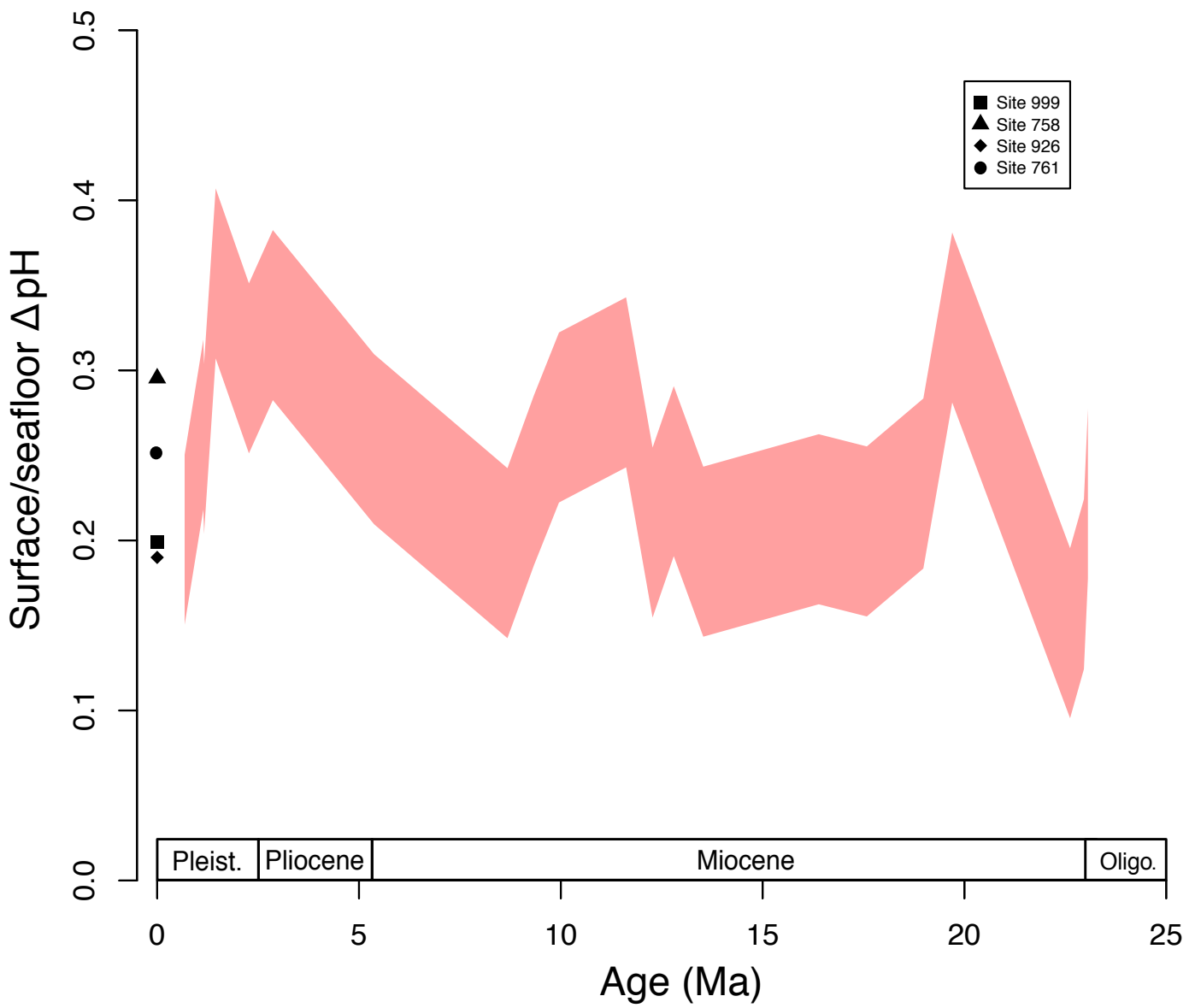


Figure 9

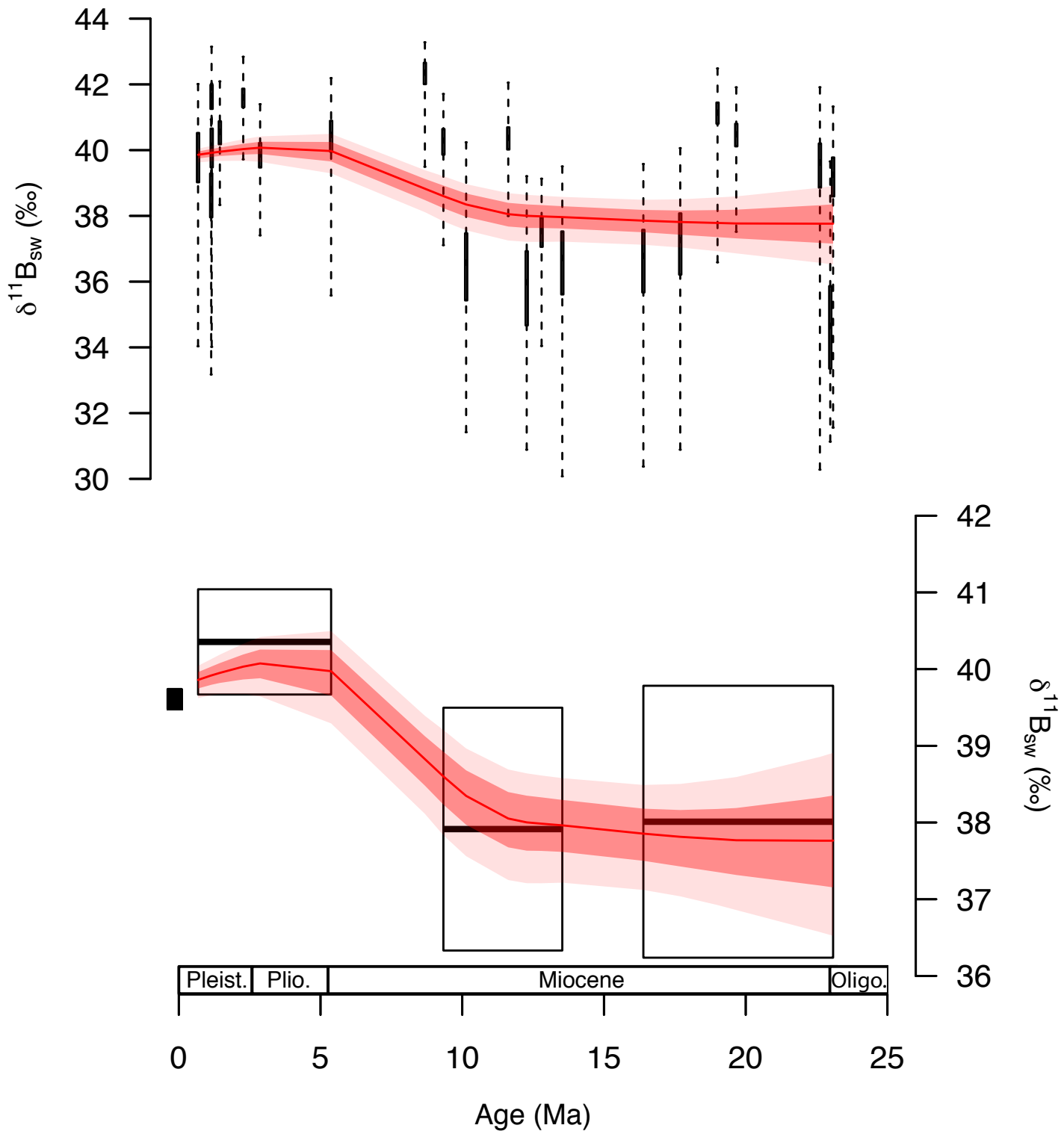


Figure 10

Figure 11

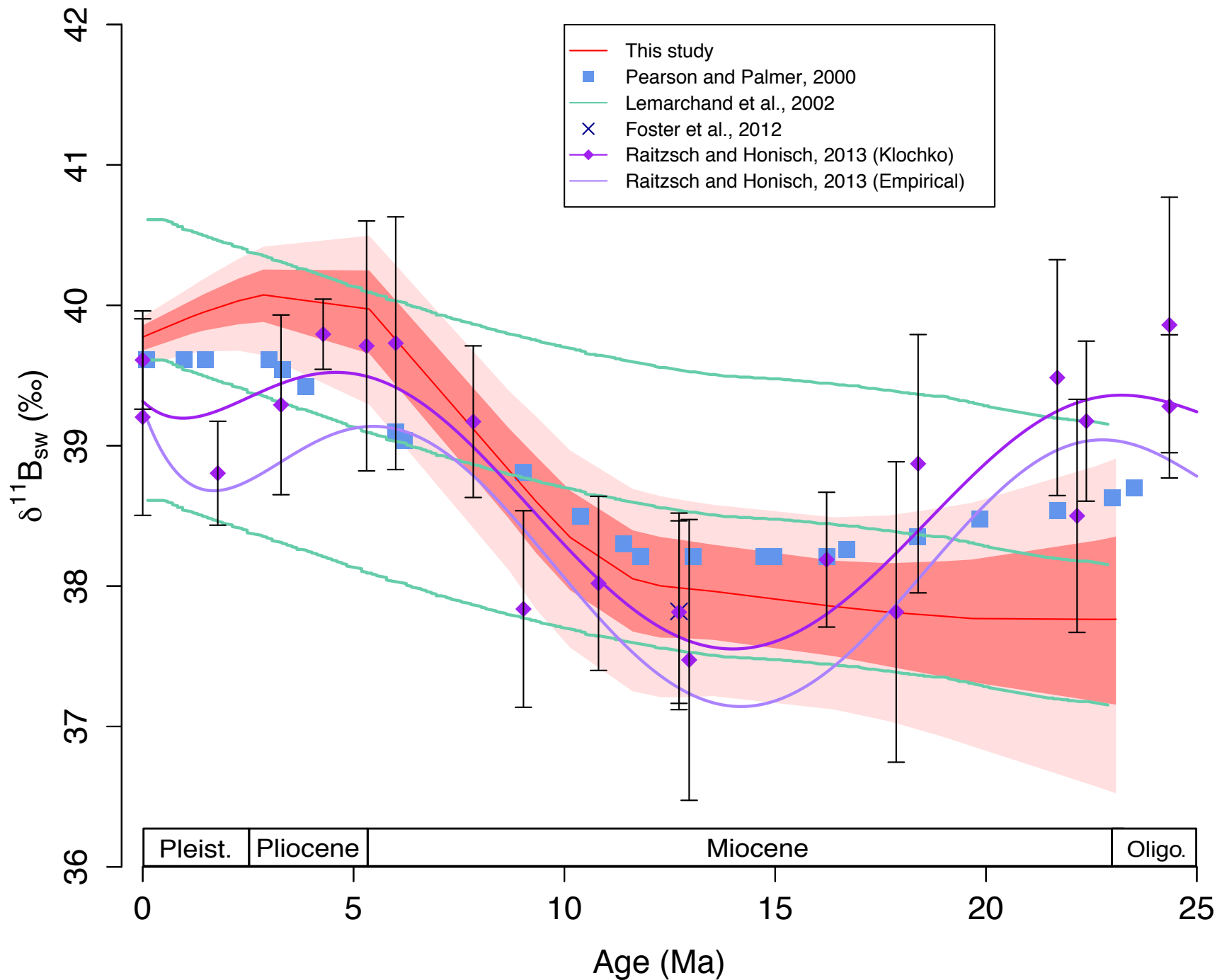
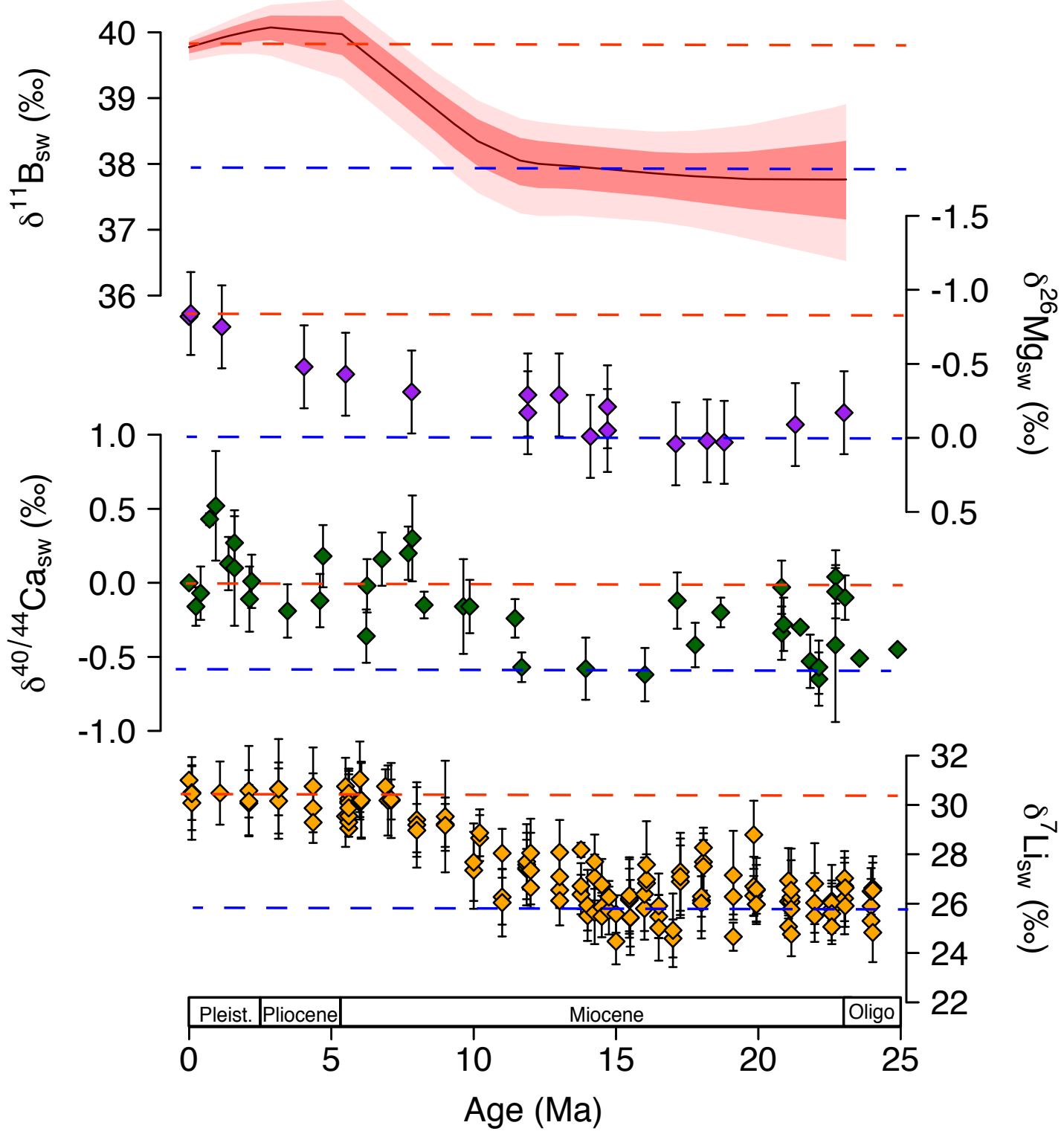


Figure 12



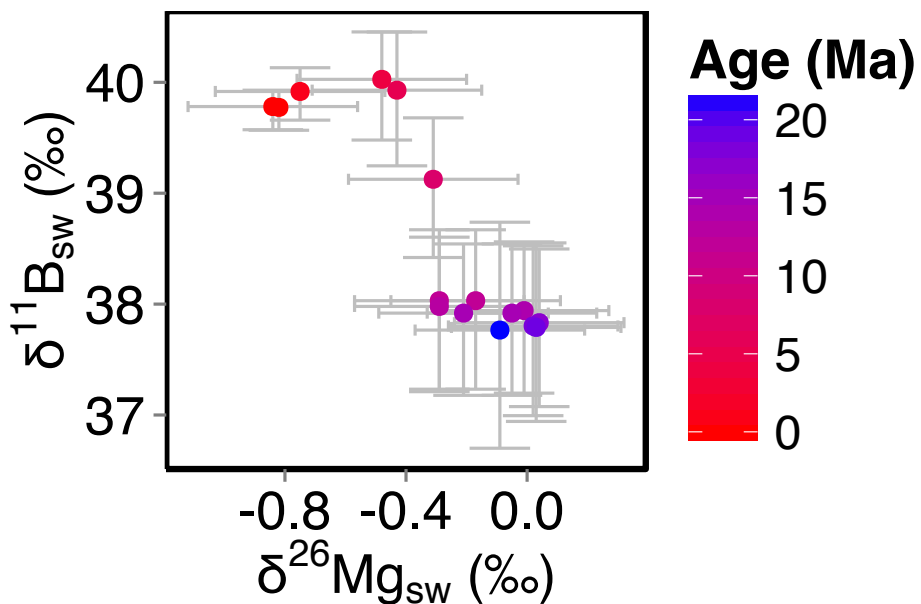
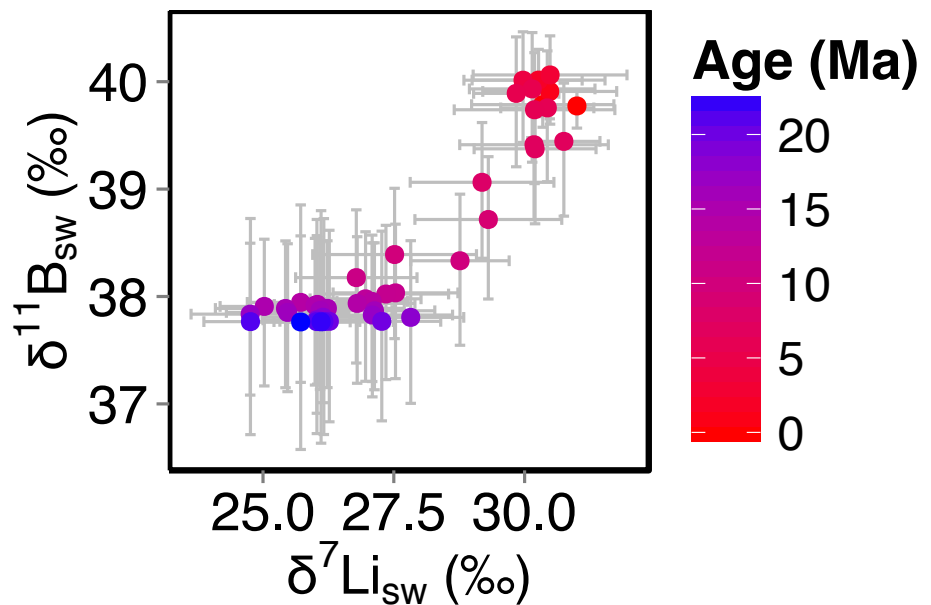
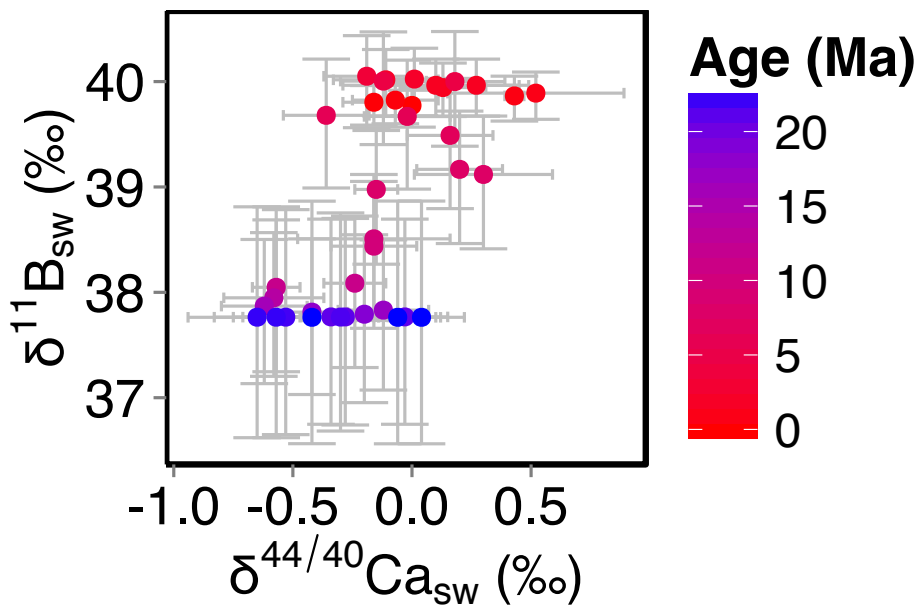


Figure 13

Table 1. CYCLOPS model parameter values defining the ensemble of 13,500 simulations*

Parameter	Description	Values assumed
PAZ surface phosphate**	unutilized polar nutrient	1µM, 1.25µM, 1.5µM, 1.75µM, 2µM
PAZ vertical exchange**	bottom water formation	2Sv, 7.75Sv, 13.5Sv, 19.25Sv, 25Sv
SAZ surface phosphate**	unutilized polar nutrient	0.7µM, 0.825µM, 0.95µM, 1.075µM, 1.2µM
AMOC circulation scheme**	deep vs. shallow overturning	NADW, GNAIW
representative timeslice***	Age ($[Ca^{2+}]$ /CCD); calcium set outright; CCD set via riverine $CaCO_3$ flux using inverse scheme	0Myr (10.6mM, 4.65km), 9Myr (12.89mM, 4.4km), 11Myr (13.33mM, 4.9km), 16Myr (14.28mM, 4.7km), 18Myr (14.57mM, 4.25km), 20Myr (14.86mM, 4.7km)
atm. CO_2 ****	set via silicate weatherability	200ppm, 300ppm, 400ppm, 500ppm, 600ppm, 700ppm, 800ppm, 900ppm, 1000ppm

* = The six parameters assume 5, 5, 5, 2, 9 and 6 values, yielding 13,500 distinct parameter combinations

** = These parameters are intended to span the full range of ocean carbon cycling over late Pleistocene glacial-interglacial cycles, as described in more detail in Hain et al. (2010)

*** = We selected representative timeslices based on local extrema in the CCD reconstruction of Pälike et al. (2012) and we combine these with appropriate reconstructed calcium concentrations based on Horita et al. (2002). These choices are intended to capture the range of long-term steady state conditions of the open system $CaCO_3$ cycle relevant to our study interval

**** = These atmospheric CO_2 levels are chosen to span a range wider than expected for the study interval. Following silicate-weathering-feedback paradigm, long-term CO_2 is fully determined by the balance of geologic CO_2 sources and silicate weathering, whereby faster acting processes of the open system $CaCO_3$ cycle compensate relative to that CO_2 level. All else equal, high CO_2 levels, low calcium concentrations and deep CCD correspond to high bulk ocean carbon concentrations (Hain et al., 2015) with many of the individual simulations of this ensemble exceeding 4000µM DIC.

Table 2

Input parameter	Uncertainty applied	Source of uncertainty estimate
Surface to sea floor ΔpH	Uniform +/- 0.05 pH units	Plausible range of $\Delta\text{pH}/\Delta\delta^{13}\text{C}$ in CYCLOPS and GENIE sensitivity tests; prediction error of linear $\Delta\text{pH}/\Delta\delta^{13}\text{C}$ regression in GENIE
$\delta^{11}\text{B}$ measurement	0.15-0.61‰	Long-term external reproducibility
Temperature	$\pm 2^\circ\text{C}$	Uncertainty in the Mg/Ca measurement and Mg/Ca-temperature calibration
Salinity	$\pm 2 \text{ psu}$	In the absence of a salinity proxy this uncertainty is applied to cover variations through time.
Seawater [Mg]	$\pm 4.5 \text{ mmol/kg}$	following Horita et al., (2002)
Seawater [Ca]	$\pm 4.5 \text{ mmol/kg}$	following Horita et al., (2002)

Table 3

Sources	Isotopic Ratio			
Oceanic Inputs	$\delta^{11}\text{B}_{\text{sw}}$ 39.61 ‰	$\delta^7\text{Li}_{\text{sw}}$ 31 ‰	$\delta^{26}\text{Mg}_{\text{sw}}$ -0.83 ‰	$\delta^{44/40}\text{Ca}_{\text{sw}}$ 0 ‰
Input from hydrothermal	6.5 ^a	8.3 ^b	N/A	-0.96 ^h
Fluid from accretionary prisms	25 ^a	15 ^b	N/A	N/A
Riverine Inputs	10 ^a	23 ^b	-1.09 ^d	-1.28 ^h
Groundwater	N/A	N/A	-0.82 ^d	-1.02 ⁱ
Outputs				
Precipitation into carbonates	20 ^a	29 ^c	-3.5 ^{d,e,f}	-1.15 ^{h,j}
Ocean crust alteration	4 ^a	15 ^b	-0.83 ^{d,g}	-1.2 ^h
Absorption onto sediment	15 ^a	15 ^b	??	N/A